# Chapter 2

## Synthesis & Characterization of

- **MCM-41**
- **12-tungstophosphoricacid anchored to MCM-41 (TPA/MCM-41)**

  **&**
- **12-tungstosilicicacid anchored to MCM-41 (TSA/MCM-41)**

- **Papers published**

  **Green Chem lett Rev, 5 (2012) 161-171**
  ***Ind. Eng. Chem. Res., 50* (2011), 13693–13702.**

*Green Chemistry Letters and Reviews*
Vol. 5, No. 2, June 2012, 161–171

Taylor & Francis
Taylor & Francis Group

## RESEARCH LETTER

# An efficient green catalyst comprising 12-tungstophosphoric acid and MCM-41: synthesis characterization and diesterification of succinic acid, a potential bio-platform molecule

Varsha Brahmkhatri and Anjali Patel*

*Faculty of Science, Department of Chemistry, M. S. University of Baroda, Vadodara 390002, India*

*(Received 13 October 2010; final version received 19 May 2011)*

An efficient green catalyst comprising 12-tungstophosphoric acid (TPA) and MCM-41 was synthesized. The catalytic activity was evaluated for liquid phase solvent free diesterification of succinic acid. The support and the synthesized catalyst were characterized by various physico-chemical techniques. Fourier transform infrared, diffuse reflectance spectroscopy, and $^{31}P$ NMR spectra indicate that the Keggin structure of TPA was not destroyed after anchoring to MCM-41. X-ray diffraction, scanning electron microscopy, and transmission electron microscopy show that TPA is uniformly dispersed inside the channels without disturbing the hexagonal array of MCM-41. The present contribution reports solvent free diesterification of succinic acid with alcohols under mild reaction conditions. The catalyst shows higher activity toward diester, especially for dioctyl succinate 99% yield was obtained with very high turnover number, $12.43 \times 10^4$. Also the catalyst shows potential of being used as recyclable catalytic material after simple regeneration without loss of any catalytic activity.

I&EC research
Industrial & Engineering Chemistry Research

ARTICLE

pubs.acs.org/IECR

# Synthesis and Characterization of 12-Tungstosilicic Acid Anchored to MCM-41 as well as Its Use as Environmentally Benign Catalyst for Synthesis of Succinate and Malonate Diesters

Varsha Brahmkhatri and Anjali Patel*

Department of Chemistry, Faculty of Science, M. S., University of Baroda, Vadodara 390002, India

**ABSTRACT:** 12-Tungstosilisic acid anchored to MCM-41 was synthesized and characterized by various physicochemical techniques such as thermogravimetric analysis (TGA), Fourier transform infrared (FT-IR), laser-Raman spectroscopy, diffuse reflectance spectroscopy (DRS), $N_2$ adsorption−desorption, $^{29}$Si-magic-angle spinning (MAS) NMR, X-ray diffraction (XRD), scanning electron microscopy (SEM), and transmission electron microscopy (TEM). The total acidity was determined by *n*-butyl amine titration. The types of acidic sites (acidic strength) were determined by potentiometric titration. The use of synthesized material was explored for esterification of diacarboxylic acids with butanol. Influence of various reaction parameters (catalyst concentration, acid/alcohol molar ratio and reaction time) on catalytic performance was studied. The catalyst shows high activity in terms of higher yields toward diesters, especially for dioctyl succinate and dioctyl malonate. The catalyst was also regenerated and reused for four cycles. All these characteristics imply the high potential of an environmentally benign catalyst for synthesis of succinate and malonate diesters.





dx.doi.org/10.1021/ie201447y | *Ind. Eng. Chem. Res.* 2011, 50, 13693–13702

**SYNTHESIS**

Heterogeneous catalysis is endlessly fascinating and still continues to be deeply mysterious. More than 90% of the chemical manufacturing processes in use throughout the world utilize catalysts in one form or another: much of the food we eat and the medicines we take , many of the fabrics and building materials that keep up warm, and almost all the fuels that transport us by road or air are produced by heterogeneously catalyzed reactions. The science and technology of the catalysis are therefore of central practical importance.

In order to contribute in this respect, heterogeneous catalysts were synthesized based on HPAs and mesoporous silica materials. Among the Keggin HPAs, TPA and TSA were selected, as TPA is the most important from the view point of stability and acidity and TSA is the next acidic and stable one in the series. Catalysis by "Anchored HPAs" has been greatly expanded during the last few years from the view point of their variety of structures and compositions. They provide the opportunities for tuning their chemical properties, such as acidities, and reactivities by choice of appropriate support.

Mesoporous silica materials, MCM-41 and SBA-15 were selected as supports. The main objective/reason of selecting them as a support are:

- They possess a series of attractive features, such as high surface area, narrow pore size distribution and high adsorption capacities which enable them to be used as catalytic "Supports".

- As well as having a highly ordered distribution of mesopores, MCM-41 and SBA-15 materials offer the possibility of incorporating catalytic active species into their structures, which improves their hydrothermal stability and produces active sites, thus broadening their field of applications[1].

- This basic structural chemical feature of the mesoporous materials would allow processing of large molecules and the eventual accommodation of intermediate transition states which are too bulky to exist within the cavities and voids of zeolites [2].

Generally mesoporous silica, MCM-41 and SBA-15 are synthesized by hydrothermal procedures as mentioned earlier. Developing a non-hydro thermally synthesis for these materials will be interesting due to the mild conditions and easily fascinating approach. Since the traditional hydrothermal procedures have some disadvantages, such as the obligatory crystallization time and high ageing temperature [3].

The present chapter describes synthesis and physico-chemical and spectroscopic characterization of support, MCM-4 and two series of catalysts, TPA and TSA anchored to MCM-41. The support and the catalysts were characterized by different physico-chemical techniques such as elemental analysis (EDS), thermo gravimetric analysis (TGA), Fourier Transform Infrared Spectroscopy (FT-IR), Laser-Raman Spectroscopy, Diffuse Reflectance Spectroscopy (DRS), X-ray diffraction (XRD), surface area measurement (BET method), pore size, pore volume and $^{31}P$ and $^{29}Si$ MAS- NMR studies. Further, the surface morphology of support and catalyst was studied by Scanning Electron Microscopy (SEM) and Transmission Electron Microscopy (TEM). The total acidity was determined by n-butylamine titration. The types of acidic sites (acidic strength) were determined by potentiometric titration.

To study the effect of pore diameter pore expanded MCM-41 was also synthesized. TPA was anchored to pore expanded MCM-41. The supports as well as the catalysts were characterized for some of the techniques such as FT-IR, low angle XRD, $N_2$ sorption isotherms, SEM and TEM as our objective was to study the effect of support pore diameter on catalytic activity of TPA.

## 2.1 EXPERIMENTAL

*Materials*

All chemicals used were of A.R. grade. $H_3PW_{12}O_{40}$. $nH_2O$ ,$H_4SiW_{12}O_{40}$. n $H_2O$ , and Cetyl triethyl ammonium bromide (CTAB) (Loba chemie, Mumbai). Tetraethylorthosilicate (TEOS) and NaOH was used as received from Merck.

**(a)Synthesis of MCM-41**

MCM-41 was synthesized using non-hydrothermal procedure reported by Q. Cai et al [4] with slight modification. Surfactant (CTAB) was added to the very dilute solution of NaOH with stirring at 60 $^0$C. When the solution became homogeneous, TEOS was added drop wise and the obtained gel was aged for 2h. The resulting product was filtered, washed with distilled water, dried at room temperature. The obtained material was calcined at 555 $^0$C in air for 5 h and designated as MCM-4. A schematic representation for synthesis of MCM-41 is shown in figure 14.

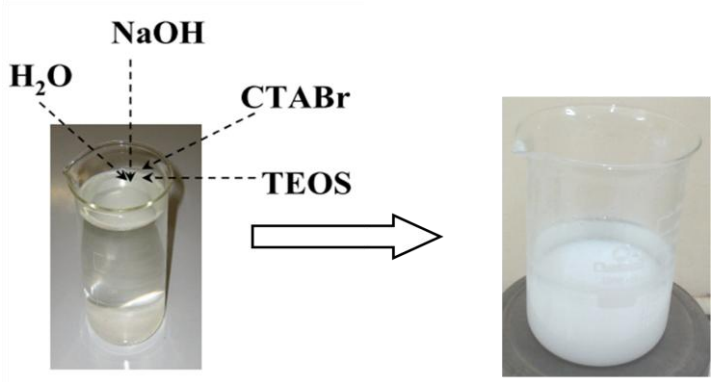


**Figure 14**. Synthesis of MCM-41.

**(b)Synthesis of the Catalysts**

**(i) Anchoring of TPA to MCM-41 (TPA/MCM-41)**

TPA was anchored to MCM-41 by incipient wetness method. 1g of MCM-41 was impregnated with an aqueous solution of TPA (0.1g/10 mL of double distilled water). The water from the suspension was allowed to evaporate at 100°C in an oven. Then the resulting mixture was dried at 100°C with stirring for 10h. The material thus obtained was designated as $TPA_1$/MCM-41. Same procedure was followed for the synthesis of a series of TPA anchored catalyst (0.2 - 0.4g/20 - 40mL of conductivity water). The obtained materials were designated as $TPA_2$/MCM-41, $TPA_3$/MCM-41 and $TPA_4$/MCM-41 respectively.

**(ii) Anchoring of TSA to MCM-41 (TSA/MCM-41)**

TSA was anchored to MCM-41 by incipient wetness method. 1g of MCM-41 was impregnated with an aqueous solution of TSA (0.1g/10 mL of double distilled water). The water from the suspension was allowed to evaporate at 100°C in an oven. Then the resulting mixture was dried at 100°C with stirring for 10h. The material thus obtained was designated as $TSA_1$/MCM-41. Same procedure was followed for the synthesis of a series of TSA anchored catalyst (0.2 - 0.4g/20 - 40mL of conductivity water). The obtained materials were designated as $TSA_2$/MCM-41, $TSA_3$/MCM-41 and $TSA_4$/MCM-41 respectively.

## CHARACTERIZATION

Characterization is a central aspect of catalyst development [5-7]. The elucidation of the structures, compositions, and chemical properties of both the solids used in heterogeneous catalysis and the adsorbates and intermediates present on the surfaces of the catalysts during reaction is vital for a better understanding of the relationship between catalyst properties and catalytic performance[5].

In case of supported catalysts, it is crucial to know if the active ingredient is on the surface of the support or diffuse in it. As a result from the scientific point of view, the investigation of the surface composition as well as local structure of catalyst at the atomic level and the correlation of these data with catalyst performance is very important in the catalytic reaction. The basic information on the structure-catalytic property relationship for catalyst systems will ultimately be of value in the design of new efficient catalysts [8]. Heterogeneous catalyst can be characterized by various tools which comprise different physic-chemical and spectroscopic techniques that are summarized in block diagram shown in figure 15.

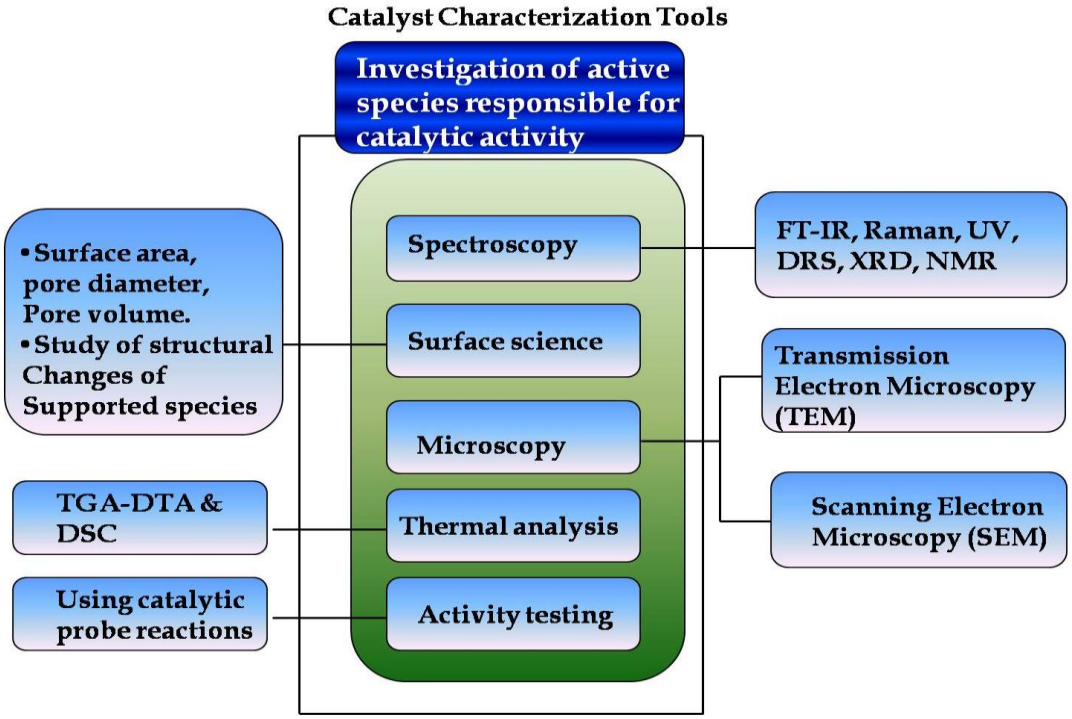


**Figure15.** Block diagram of various techniques used in characterization of catalyst

During the last few years many techniques for determining chemical composition, electronic properties and the structure of the upper atomic layers of solids have reached maturity.

The available analytical techniques can be classified into broad categories based on the information obtained by them.

1. Spectroscopic methods which include the study of structural aspects of the supported species as well as stability of supported species.

2. Study of surface area, pore volume, particle diameter, particle size distribution, dispersion of the catalyst species as well as any structural change of supported species onto the surface of the support.

Spectroscopy is a non-destructive method of analysis and provides information on the types of atoms present on surfaces, how are they influenced by adsorbed species, precise adsorption sites of atoms and molecules, their bond strengths, lengths and angles, and the influence of surface chemical bond on surface reactivity.

In the present chapter supports and the catalysts were characterized by various physico-chemical techniques such as TGA-DTG, FT-IR, Laser-Raman Spectroscopy, DRS, $N_2$ adsorption-desorption, $^{29}Si$-MAS NMR, XRD, SEM and TEM. The total acidity was determined by n-butyl amine titration. The types of acidic sites (acidic strength) were determined by potentiometric titration.

**Elemental Analysis**

**Energy-dispersive X-ray spectroscopy (EDS or EDX) [9]**

EDS or EDX is an analytical technique used for the elemental analysis or chemical characterization of a sample. It is one of the variants of X-ray fluorescence spectroscopy which relies on the investigation of a sample through interactions between electromagnetic radiation and matter, analyzing X-rays emitted by the matter in response to being hit with charged particles. Its characterization capabilities are due in large part to the fundamental principle that each element has a unique atomic structure allowing X-rays that are characteristic of an element's atomic structure to be identified uniquely from one another.

To stimulate the emission of characteristic X-rays from a specimen, a high-energy beam of charged particles such as electrons or protons, or a beam of X-rays, is focused into the sample being studied. At rest, an atom within the sample contains ground state (or unexcited) electrons in discrete energy levels or electron shells bound to the nucleus. The incident beam may excite an electron in an inner shell, ejecting it from the shell while creating an electron hole where the electron was. An electron from an outer, higher-energy shell then fills the hole, and the difference in energy between the higher-energy shell and the lower energy shell may be released in the form of an X-ray (figure 16). The number and energy of the X-rays emitted from a specimen can be measured by an energy-dispersive spectrometer. As the energy of the X-rays are characteristic of the difference in energy between the two shells, and of the atomic structure of the element from which they were emitted, this allows the elemental composition of the specimen to be measured.

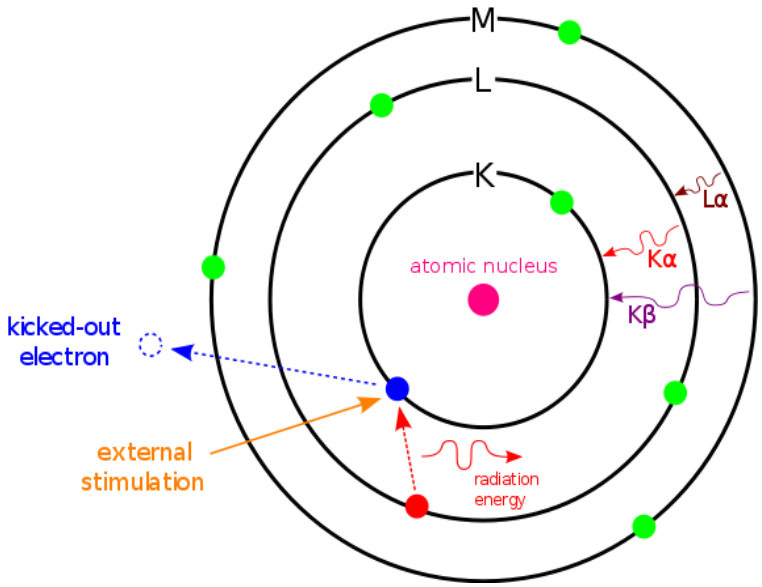


**Figure16.** Phenomenon of EDX absorption

The elemental analysis was carried out using JSM 5610 LV combined with INCA instrument for EDX-SEM analyzer for the quantitative identification of metal ions.

**Thermo Gravimetric Analysis (TGA) [10]**

It is a technique whereby the weight of a substance, in an environment heated or cooled at a controlled rate, is recorded as a function of time or temperature.

The temperature-weight loss profile of a supported catalyst can provide important quantitative information on the types of water present in the sample. It is usually possible to distinguish loosely held "physisorbed" water from strongly bonded "chemisorbed" water and helps determine the best conditions for removing the former.

The loss of water from supported catalysts at temperature greater than $300^0$C is probably due to surface dehydroxylation, which may be encouraged by the catalyst. Loss or decomposition of the catalyst can also be followed by TGA.

More usefully, the study of the decomposition of less stable catalysts can also be done which help in determine the maximum activation temperatures and the temperatures at which the supported reagents can be safely used in reactions.

TGA measurements were carried out on the Mettler Toledo Star SW 7.01 in the temperature range 40 $^{o}$C to 600 $^{o}$C. All measurements were carried out under nitrogen atmosphere with a flow rate of 2 ml/ min and a heating rate of 10$^{o}$ C/ min.

**Fourier Transform Infrared Spectroscopy (FT-IR) [9]**

FT-IR spectroscopy is probably the most useful and widely used technique to study supported reagents. It provides the following information.

1. Identification of the surface species;
2. Dispersion of the reagent over the support surface;
3. Surface activity studies with the use of probe molecules;

The most common ways of studying an insoluble solid are: 1) as a mull; 2) as a disc; and 3) directly as a powder. These methods differ in terms of degree of difficulty (in obtaining useful spectra), ease of sample preparation, and reliability of the information obtained.

Both the mull and disc methods are transmittance techniques. FT-IR opaque or highly scattering materials may not be suitable for analysis by transmission spectroscopy. In cases such as these the diffuse reflectance method can be a very useful alternative. This involves irradiating a powdered sample, then measuring the spectrum of a non-absorbing standard such as KCl or KBr. Diffuse reflectance is generally a qualitative IR technique but it can be used as a quantitative technique if the sample and dilution matrix meet certain criteria such as

1. There must be negligible specular reflectance
2. The sample must be dilute
3. Scattering coefficient should be constant both as concentration is varied and across the whole spectrum.

Both scattering and specular reflectance are affected by particle size therefore, a uniform and reproducible particle size is important if reliable quantitative information is to be derived from spectra.

FT-IR absorption spectra of various catalysts were recorded on a FT-IR Perkin Elmer instrument at room temperature using KBr pellets in the range of 4000 $cm^{-1}$ to 400 $cm^{-1}$. The powdered samples were ground with KBr in 1: 10 ratio and pressed (5 $ton/cm^2$) for making the pellets. The data were collected at an average of 25 scans.

**Laser Raman spectroscopy (LRS) [11]**

Raman spectroscopy (named after Sir C. V. Raman) is a spectroscopic technique used to study vibrational, rotational, and other low-frequency modes in a system. It relies on inelastic scattering, or Raman scattering, of monochromatic light, usually from a laser in the visible, near infrared, or near ultraviolet range.

Raman spectroscopy is a useful technique for the identification of a wide range of substances - solids, liquids, and gases. It is a straightforward, non-destructive technique requiring no sample preparation. Raman spectroscopy involves illuminating a sample with monochromatic light and using a spectrometer to examine light scattered by the sample.

Most Raman spectrometers for material characterization use a microscope to focus the laser beam to a small spot (<1-100mm diameter). Light from the sample passes back through the microscope optics into the spectrometer. Raman shifted radiation is detected with a charge-coupled device (CCD) detector, and a computer is used for

data acquisition and curve fitting. These factors have helped Raman spectroscopy to become a very sensitive and accurate technique.
The Raman spectra were recorded on a FT-Raman Spectrophotometer Model Bruker FRA 106.

**Diffuse Reflectance Spectra (DRS)**

The DRS of sample were recorded at room temperature on Perkin Elmer 35 LAMDA instrument using barium sulphate as a reference. $BaS0_4$ was used as a reference. Even though the background was measured independently of the sample the measurements were always performed in double beam mode to compensate for instabilities.

**Solid state MAS-NMR ($^{31}P$ & $^{29}Si$) [12]**

Nuclear Magnetic Resonance (NMR), since its discovery in 1946, as a technique for the precise determination of magnetic moments of nuclei by physicists has undergone major developments to become one of the most important tools in all branches of science such as chemistry, biology, agriculture and medicine. One can say that it finds applications literally from "molecules to man". The availability of high field superconducting magnetic has further improved the sensitivity in addition to the resolution. Further developments in the field stem from the introduction of the various multipulse techniques which enable the systems to be studied in various phases of matter viz., liquid, liquid crystalline and solid. The introduction of 2-dimentional techniques is responsible for the study of more complex molecules.

The chemical shift and the coupling constants provide information on the static as well as dynamic properties of molecules. The presence and the absence of the functional groups and their quantitative estimation can be made from the chemical

shifts. The coupling constants provide information on the molecular structure and conformation. The function and interaction of the molecules can also be studied by both the chemical shifts and the coupling constants. The chemical exchange, hydrogen bonding and other weak molecular interactions can all be studied by NMR.

In nuclear magnetic resonance, **magic angle spinning** (MAS) is a technique often used to perform experiments in solid-state NMR spectroscopy.

By spinning the sample (usually at a frequency of 1 to 70 kHz) at the magic angle $\theta_m$ (ca. 54.74°, where $\cos^2\theta_m=1/3$) with respect to the direction of the magnetic field, the normally broad lines become narrower, increasing the resolution for better identification and analysis of the spectrum.

The chemical shifts of peaks in solid state $^{31}P$ and $^{29}Si$ NMR spectra were used for characterization of solid materials. The magic- angle spinning (MAS) solid state NMR studies was carried out on a Bruker Avance DSX-300 NMR spectrometer under ambient conditions. The $^{31}P$ MAS NMR spectra were recorded at 121.48 MHz using a 7 mm rotor probe with 85% phosphoric acid as an external standard. The spinning rate was 4 – 5 kHz. Catalysts after treatment were kept in a desiccator over $P_2O_5$ until the NMR measurement. The $^{29}Si$ NMR spectra were recorded at 121.49 MHz using a 7 mm rotor probe, number of acquisitions AQ: 0.0048888 Sec and spinning rate of 5-7 kHz, with TMS as an external standard.

**Powder X-Ray Diffraction (XRD) [9]**

At the simplest level, XRD can be used to confirm "reasonable" reagent dispersion over the surface of the support. For supported reagents containing low % by weight of the reagent, the absence of diffraction lines due to the reagent or the presence of only very weak lines can be taken to indicate that most of the reagent is present in the form of extremely small crystals and/or is highly dispersed.

XRD can be used similarly to detect poorly dispersed or macro-crystalline reagent. In principle, XRD can be used to give quick information on the efficiency of dispersion of any supported reagent where the reagent normally exists in the crystalline state. XRD may also be useful for the identification of species formed during the preparation on subsequent chemistry of a supported reagent. This can be especially useful for unstable reagents, corrosive reagents and where the supported reagent has been subject to high-temperature thermal treatment. XRD has also been used to characterize the nature of surface species.

The powder X Ray Diffraction pattern of support and supported catalysts was obtained by using the instrument Philips Diffractometer (Model PW - 1830). The conditions used were Cu Kα radiation (1.5417 Å), scanning angle from 0° to 80°.

**BET Measurement [10]**

In case of catalysis, especially, heterogeneous catalysis the reaction follows the surface adsorption phenomenon rather than the typical bulk type catalysis. Hence, the catalytic surfaces need to be characterized by their physical properties.

Since the catalytic action occurs at specific sites on solid surfaces, often called 'active sites', the rate can be significantly increased by using a very high surface area catalyst. It is generally believed that higher the surface area of a catalyst, higher will be the activity.

As surface area of the catalyst is directly proportional to the catalytic activity of the heterogeneous catalysts, the measurement of the surface area is most important study for the same. Further from the surface area, one can get the information on the pore volume, pore size which will be helpful to understand the mechanism of the reaction occurs.

Apart from surface area measurements, determination of pore size distribution is an equally important parameter. For a given catalyst, the distribution of pore sizes may be such that some of the catalyst is completely inaccessible to large molecules and may restrict the rate of conversion of products by controlling the diffusion of reactant in the internal pore structure. The standard method for measuring catalyst areas and pore size are based on the physical adsorption of gas on the solid surface.

Surface area and pore size distribution of various catalysts were measures according to Brunauer-Emmett-Teller (BET) method, involving nitrogen adsorption-desorption using Carlo-Erba sorptometer (Model: Series 1800). From the adsorption desorption isotherms specific surface area was calculated using BET method. The samples were degassed under vacuum (5 – 10.3 mmHg) at 120 °C for 4 h, prior to measurement, to evacuate the physiosorbed moisture. Further the pore size distributions were calculated applying the Barrett-Joyner-Halenda (BJH) method to the desorption branches of the isotherm.

**Scanning Electron Microscopy (SEM) [9]**

SEM provides morphological and topological information about the surfaces of solids that is usually necessary in understanding the behavior of the surfaces. SEM is often the first step in the study of the surface properties of a solid material. The surface of a solid sample is swept in a raster pattern with a finely focused beam of electrons or with a suitable probe. The surface morphology of the support and the anchored HPAs were studied.

SEM has been used successfully to study reagent dispersion and surface morphologies. SEM can prove to be more sensitive technique than XRD to study reagent dispersion.

The surface morphology of the supports as well as supported catalysts was studied by Scanning Electron Microscopy using a Jeol SEM instrument (Model-JSM-5610 LV) with scanning electron electrode at 15 kV. Scanning was done at 1 mm range and images taken at a magnification of 100X for $ZrO_2$ and 100X and single particle image at 500X for supported catalysts.

**Transmission Electron Microscopy (TEM) [13]**

TEM images are formed using transmitted electrons (instead of the visible light) which can produce magnification details up to 1,000,000 x with resolution better than 10A$^o$. The images can be resolved over a fluorescent screen or a photographic film. Furthermore the analysis of the X-ray produced by the interaction between the accelerated electrons with the sample allows determining the elemental composition of the sample with high spatial resolution.

In TEM, the transmission of electron beam is highly dependent on the properties of material being examined. Such properties include density, composition, etc. For example, porous material will allow more electrons to pass through while dense material will allow less. As a result, a specimen with a non-uniform density can be examined by this technique.

TEM was done on JEOL (JAPAN) TEM instrument (model-JEM 100CX II) with accelerating voltage 220 kV. The samples were dispersed in ethanol and ultra-sonicated for 5-10 minutes. A small drop of the sample was then taken in a carbon coated copper grid and dried before viewing.

**Acidity measurement**

A complete description of the surface acid properties of a solid involve the determination of the acid strength of the sites, their density (number of acid centers per unit surface area of the solid), and their nature (Bronsted or Lewis type). Such descriptions are not easy to make, as the strength and the density of the sites are generally strictly connected to each other and besides the distribution of the acid strength is usually heterogeneous.

According to Walling, the acid strength of a solid can be defined as its ability to convert a neutral base, adsorbed on its surface, into the corresponding conjugated acid.

The number of acid centers present on a solid surface is usually expressed as surface density, e.g., as the number of centers, or mmoles, per unit weight or unit surface area.
The different types of methods used for the total acidity measurement are as follows:

1. **Non aqueous titration [14]**
2. **Hammett Acidity (Total acidity) [10]**
3. **Temperature-Programmed Desorption (TPD) of Chemisorbed Bases [14]**
4. **Total acidity determination by n-butyl amine titration [15]**
5. **Determination of acidic strength [15]**

We have used n-butyl amine titration method for the determination of total acidity. Also the potentiometric titration with n-butyl amine was used to determination of acidic strengths which are described here.

**Total acidity determination**

The total surface acidity for all the materials has been determined by n-butylamine titration [16]. A 0.025M solution of n-butylamine in toluene was used for estimation. The catalyst weighing 0.5 gm was suspended in this solution for 24h and excess base was titrated against trichloroacetic acid using neutral red as an indicator. This gives the total surface acidity of the material.

**Determination of acidic strength**

The determination of the types of acidic sites and their quantification was made by potentiometric titration with 0.05N n-butyl amine in acetonitrile. A sample of 0.5 gm of the catalyst was added to 50ml of acetonitrile and the system was magnetically stirred at 25 $^{o}$C. The initial potential was measure after electrode signal stabilization. Small aliquots (0.5 ml) of 0.05N n-butyl amine in acetonitrile were added and the potential measured after stabilization of readings [17].

**(a) Characterization of the support, MCM-41**

The synthesized MCM-41 was characterized by various spectroscopic techniques. Only the main characterization techniques such as XRD, SEM, TEM and BET surface area measurements are presented here and the rest of the techniques will be discussed along with the catalyst characterization.

**X-ray Diffraction**

The XRD pattern of MCM-41 is shown in Figure 17. The XRD pattern of the calcined MCM-41 showed a sharp peak around $2\theta=2^{o}$ and few weak peaks in $2\theta=3\sim5^{o}$, which indicated well-ordered hexagonal structure of MCM-41 [18-19].

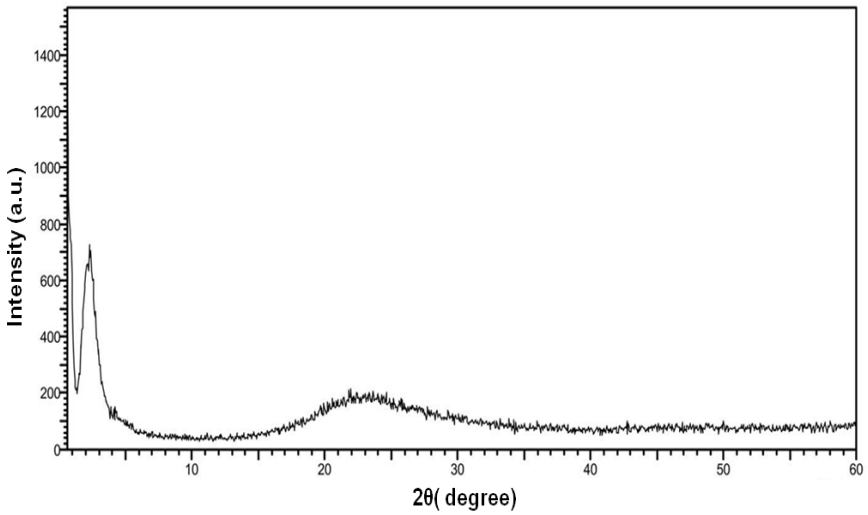


**Figure17.** XRD pattern of MCM-41

**Transmission Electron Microscopy**

TEM image of MCM-41 are shown in figure 18, which clearly shows hexagonal mesopores in MCM-41. This confirms long range order in the synthesized material, MCM-41.

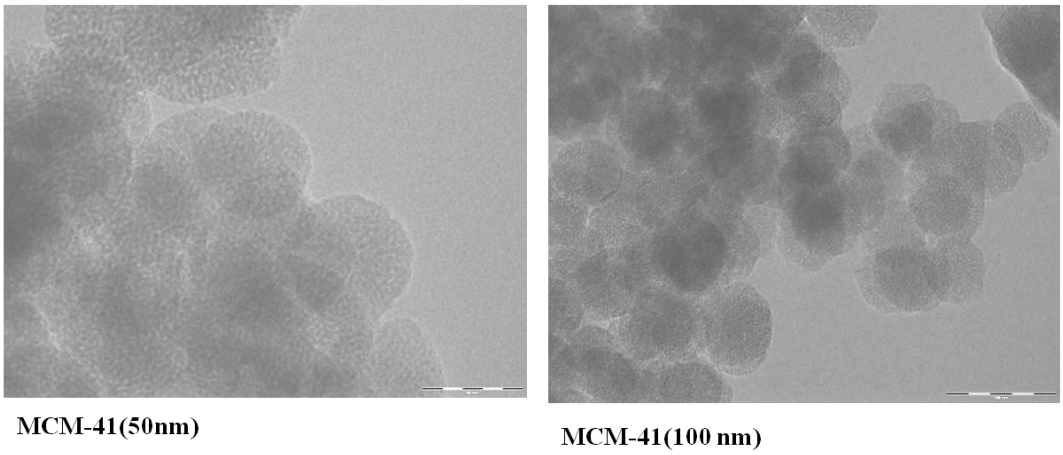


**Figure 18.** TEM images of MCM-41

**BET surface area measurements**

The surface area of MCM-41 was found to be 659 $m^2/g$ with 4.7 nm pore diameter.

**(b) Characterization of TPA/MCM-41 and TSA/MCM-41**

**Chemical Stability**

Chemical stability of a catalyst plays an important role. The materials which have a high solubility in water and/or in acidic media may not be very useful. It is advisable to have a rough guide of the solubility of the material being used as a catalyst. The stability of all the synthesized materials have to be check in different acids and bases.

The anchored catalysts were evaluated for chemical stability and the present catalysts, shows no change in color or form on heating with water. The materials are stable in different mineral acids like HCl, $H_2SO_4$, $HNO_3$ and bases like NaOH, $Na_2O_3$ etc. up to ~ 2M concentration.

**Leaching test**

Any leaching of the active species from the support makes the catalyst unattractive and hence it is necessary to study the stability as well as leaching of HPA from the support. HPA can be quantitatively characterized by the heteropoly blue colour, which is observed when it reacted with a mild reducing agent such as ascorbic acid [20]. In the present study, this method was used for determining the leaching of HPA from the support. Standard samples containing 1–5% of HPA in water were prepared. To 10 ml of the above samples, 1 ml of 10% ascorbic acid was added. The mixture was diluted to 25 ml. The resultant solution was scanned at λmax of 785 $cm^{-1}$ for its absorbance values. A standard calibration curve was obtained by plotting values of absorbance against % concentration. 1 g of catalyst with 10 ml conductivity water was refluxed for 24 h. Then 1 ml of the supernatant solution was treated with 10% ascorbic acid. Development of blue colour was not observed indicating that there was no leaching. The same procedure was repeated with alcohols and the filtrate of the reaction mixture after completion of reaction in order to check the presence of any leached HPA. The absence of blue colour indicates no leaching of HPA.

**Elemental analysis (EDS)**

EDS analysis for $TPA_3$/MCM-41 and $TSA_3$/MCM-41 catalyst is shown in table 7.The results obtained from EDS were in good agreement with the theoretical values.

**Table 7.** Elemental analysis (EDS).

| Catalyst | Elemental analysis (weight %) | | | | | |
|---|---|---|---|---|---|---|
| | | | W | | P | |
| | O | Si | By EDS | Theoretical | By EDS | Theoretical |
| $TPA_3$/MCM-41 | 53.9 | 27.8 | 18.0 | 19 | 0.30 | 0.32 |
| $TSA_3$/MCM-41 | 55.3 | 27.0 | 17.97 | 19 | - | - |

**Thermal Analysis (TGA-DTG)**

TGA of pure TPA, MCM-41 and $TPA_3$/MCM-41 is shown in Figure 19. TGA of MCM-41 shows initial weight loss of 6.14% at 100 $^oC$ .This may be due to the loss of adsorbed water molecules. The final 7.92% weight loss above 450 $^oC$ may be due to the condensation of silanol groups to form siloxane bonds. After that absence of any weight loss indicates that support is stable up to 600 $^oC$.

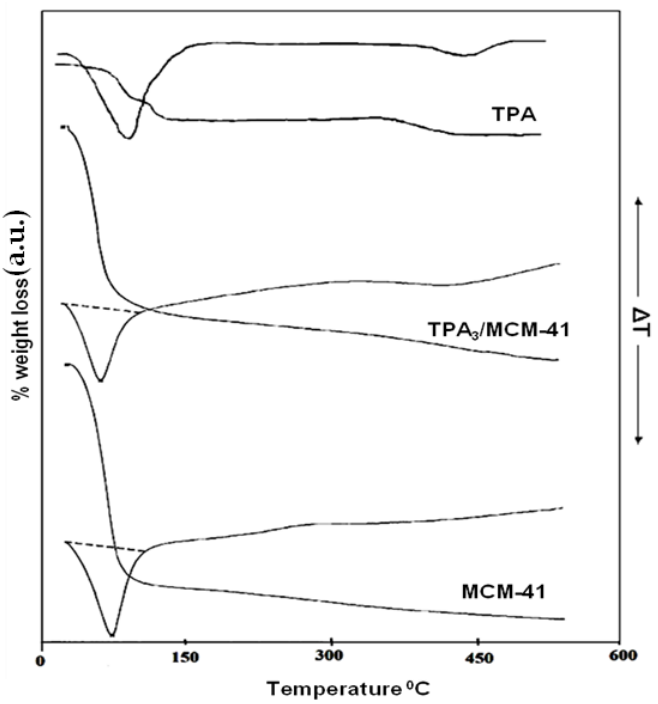


**Figure 19.** TGA-DTG of TPA, MCM-41 and $TPA_3$/MCM-41.

The unsupported pure TPA exhibits weight loss in three stages at 100, 200 and 485 °C as indicated by the DTA curve (Figure 19). These can be attributed to initial weight due to adsorbed water, second weight loss due to loss of water of crystallization near 200 °C to give the Keggin structure, which is stable on heating up to 350 °C. The endothermic peak observed on DTA curve at 485 °C may be attributed to the decomposition of the Keggin structure of TPA into the simple oxides [21].

The TGA of $TPA_3$/MCM-41 (Figure 19) shows initial weight loss of 3.6% due to the loss of adsorbed water. Second weight loss of 1.2% between 150-250 °C corresponds to the loss of water of crystallization of Keggin ion. After that another gradual weight loss was also observed from 250-500 °C due to the difficulty in removal of water contained in TPA molecules inside the channels of MCM-41. The results are in good agreement with reported one [22]. This type of inclusion causes the stabilization of TPA molecules inside the channels of MCM-41.

TGA of pure TSA, MCM-41 and $TSA_3$/MCM-41 is shown in Figure 20. The TGA of 12-tungstosilicicacid (TSA) shows 4-6% weight loss within a temperature range of 100-180$^0$C which is due to the loss of adsorbed water molecules. Further it shows 1-3% weight loss at 250-280 $^o$C due to the loss of water of crystallization and 1-3% weight loss at 470-500 $^o$C which is due to the decomposition of heteropolyacid and this is in good agreement with reported one [23].

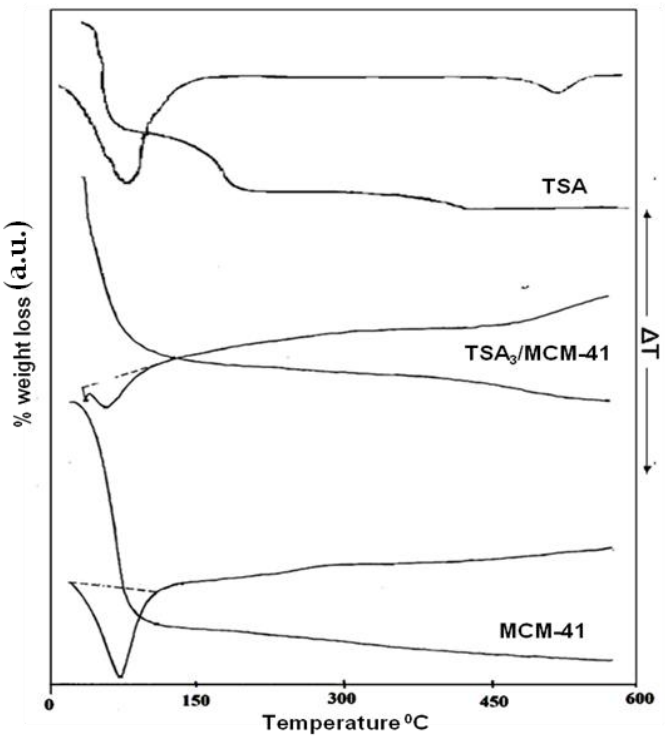


**Figure 20.** TGA-DTG TSA, MCM-41 and $TSA_3$/MCM-41

The TGA of $TSA_3$/MCM-41 shows (Figure 20) initial weight loss of 10.5% due to the loss of adsorbed water. Second weight loss of 2.8% between 150-250 $^o$C corresponds to the loss of water of crystallization of Keggin ion. After that another gradual weight loss was also observed from 250-500 $^o$C due to the difficulty in removal of water contained in TSA molecules inside the channels of MCM-41. This type of inclusion causes the stabilization of TSA molecules inside the channels of MCM-41.

**Fourier Transform Infrared Spectroscopy (FT-IR)**

FT-IR spectra of MCM-41, TPA, and $TPA_3$/MCM-41 are shown in Figure 21. FT-IR of MCM-41 (Figure 21) shows a broad band around 1300-1000 $cm^{-1}$ corresponding to asymmetric stretching of Si-O-Si. The band at 801 and 458 $cm^{-1}$ are due to symmetric stretching and bending vibration of Si-O-Si respectively. The band at 966 $cm^{-1}$ corresponds to symmetric stretching vibration of Si-OH. The broad absorption band around 3448 $cm^{-1}$ is the absorption of Si-OH on surface, which provides opportunities for forming the hydrogen bond [24].

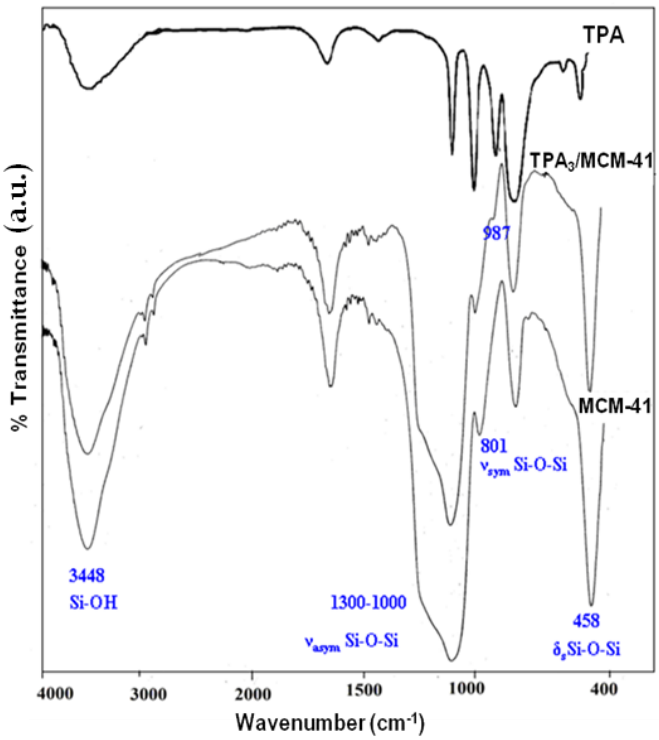


**Figure21.** FT-IR spectra of TPA, MCM-41 and $TPA_3$/MCM-41

FT-IR spectra of $TPA_3$/MCM-41 (Figure 21) is almost the same as that of MCM-41. The reported bands for TPA, at 1088 $cm^{-1}$, 987 $cm^{-1}$and 800 $cm^{-1}$ corresponding to W-O-W bending, W-O and P-O symmetric stretching respectively [25], are absent in $TPA_3$/MCM-41. If TPA is dispersed onto the surface of support, the mentioned bands for TPA should be seen in the FT-IR spectra. The lack of IR-bands of TPA may be because of too low amount of acid, or the TPA bands superimposed with those of support.

FT-IR spectra of MCM-41, TSA, and $TSA_3$/MCM-41 are shown in Figure 22. The FTIR of TSA has five characteristic bands at 1020, 980, 926, 878, and 779 $cm^{-1}$ which corresponds to $W_d$=O symmetrical and asymmetrical, Si – O asymmetrical, W–$O_b$ – W asymmetrical, and W-Oc-W asymmetrical, respectively [25].

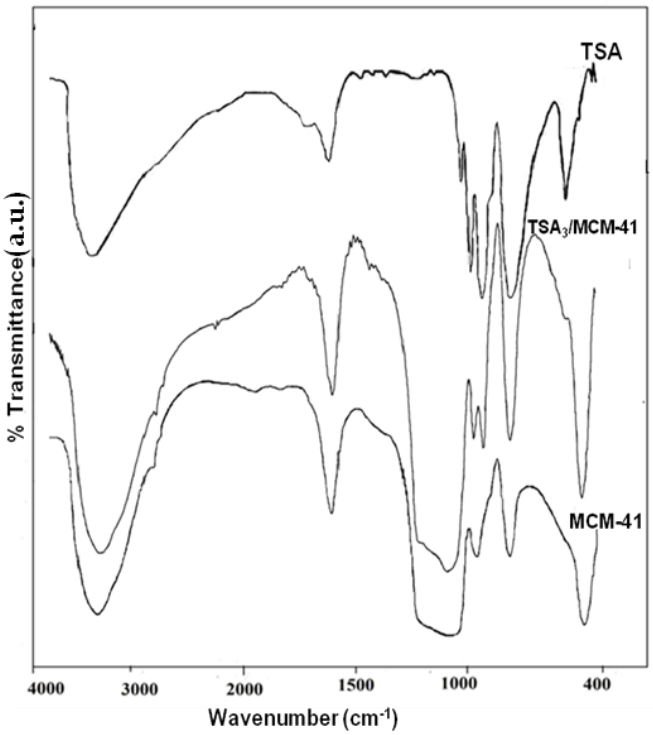


**Figure 22.** FT-IR spectra of MCM-41, TSA and $TSA_3$/MCM-41

The FT-IR spectrum of $TSA_3$/MCM-41 (Figure 22) is almost the same as that of the support, MCM-41. The typical bands for TSA, at 979 $cm^{-1}$ and 923 $cm^{-1}$, corresponding to $W_d$=O and Si – O symmetric stretching, respectively, are clearly observed in $TSA_3$/MCM-41. The presence of these bands strongly reveals that the primary structure of TSA Keggin anion is preserved even after anchoring to MCM-41 support. The absence of vibration band at 799 $cm^{-1}$ of TSA may be because of very low concentration of TSA, or the TSA bands may be superimposed with those of support.

In addition to the characteristic band for TSA, FT-IR spectra of $TSA_3$/MCM-41 also shows the infrared absorption peaks at 1637 and 3450 $cm^{-1}$ with a shoulder at 3250 $cm^{-1}$ , probably corresponding to the bending and stretching vibrations of

bridging hydroxyl, respectively, because of the interaction of TSA anions and surface silanol groups of MCM-41.

**Laser Raman Spectroscopy (LRS)**

Raman spectra of TPA and $TPA_3$/MCM-41 are shown in Figure 23. The Raman spectrum of TPA shows bands at 1010, 990, 900, 550, and 217 $cm^{-1}$ , which have already been assigned to $v_s$ (W-$O_d$ ), v as (W-$O_d$ ), $v_{as}$ (W-$O_b$-W), $v_s$ (W-$O_c$-W), and $v_s$ (W-$O_a$), respectively (Figure 23) where $O_a$, $O_b$, $O_c$ , and $O_d$ correspond to the oxygen atoms linked to phosphorus, to oxygen atoms bridging two tungsten (from two different triads for $O_b$ and from the same triad for $O_c$ ), and to the terminal oxygen W=O, respectively [26].

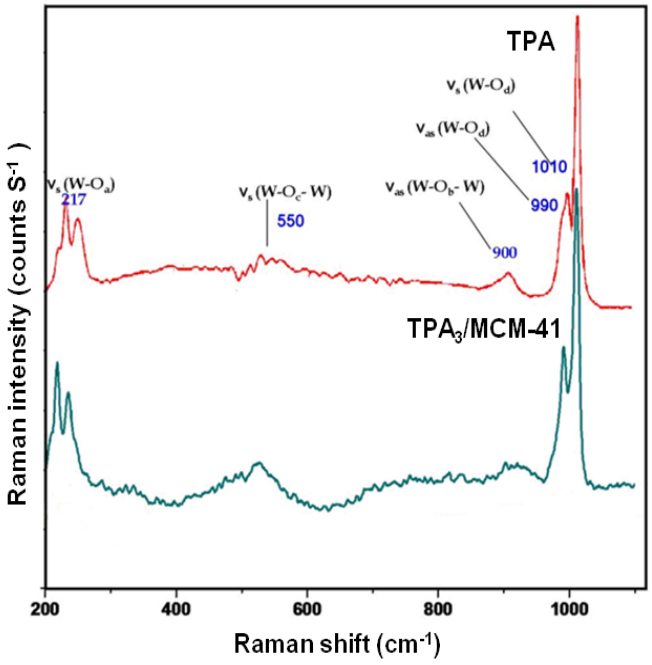


**Figure 23.** Raman spectra of TPA and $TPA_3$/MCM41

In case of anchored catalysts, $TPA_3$/MCM-41 the absence of a significant band shifts in the spectra indicates that the environment of the Keggin unit is similar to that of TPA which confirms the retainment of the Keggin structure even after anchoring to support MCM-41.

Raman spectra of TSA and $TSA_3$/MCM-41 are shown in Figure 24. The Raman spectrum of TSA shows bands at 1019, 981, 927, 881 and 785 , which corresponds to

$v_s$ (W-$O_d$ ), v as (W-$O_d$ ), v as (W-$O_b$-W), v s (W-$O_c$-W), and v s (W-$O_a$), respectively (Figure 24) where $O_a$, $O_b$, $O_c$ , and $O_d$ correspond to the oxygen atoms linked to silicon, to oxygen atoms bridging two tungsten (from two different triads for $O_b$ and from the same triad for $O_c$ ), and to the terminal oxygen W=O, respectively [27].

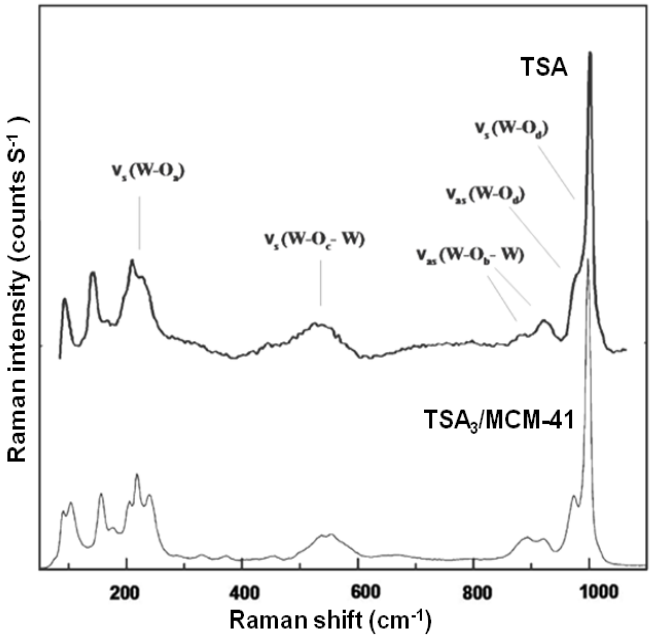


**Figure 24.** FT- Raman spectra of TSA and $TSA_3$/MCM-41

In case of anchored catalyst, $TSA_3$/MCM-41, the absence of a significant band shift in the spectra indicates that the environment of the Keggin unit is similar to that of TSA which confirms the retainment of the Keggin structure even after anchoring to support MCM-41.

**Diffuse Reflectance Spectroscopy (DRS)**

The DRS spectra of MCM-41, TPA, TSA, $TPA_3$/MCM-41 and $TSA_3$/MCM-41 are shown in Figure 25. A broad band from 260 to 275 was observed for TPA/TSA. This characteristic band can be assigned to the oxygen-metal charge transfer of heteropoly anion which is in agreement with a previous report [28]. The DRS spectra of the catalysts ($TPA_3$/MCM-41 and $TSA_3$/MCM-41) show $\lambda$max at 260 nm which is in good agreement with the earlier reported data giving evidence for the presence of the undegraded Keggin species (TPA/TSA) in MCM-41.

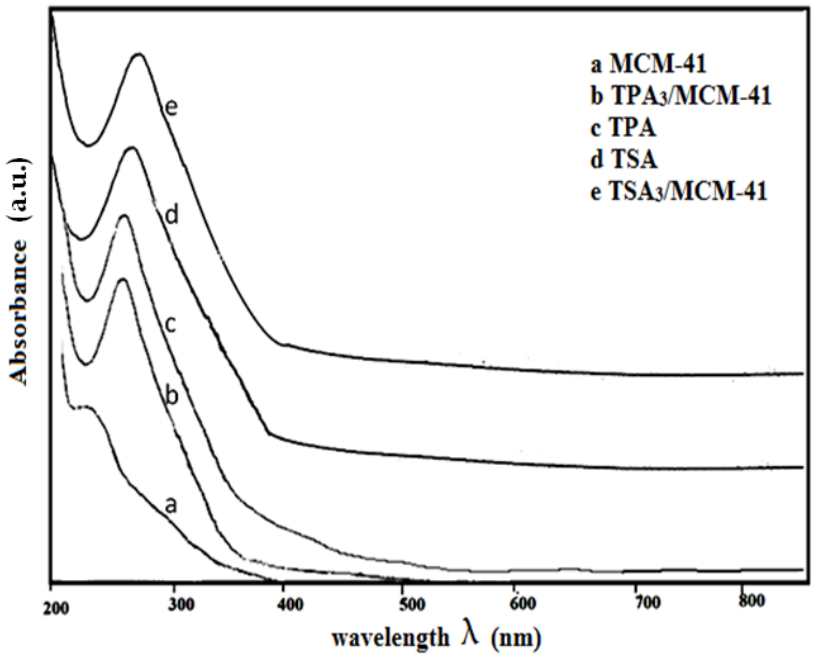


**Figure 25.** DRS of MCM-41, TPA, TSA, $TPA_3$/MCM-41 and $TSA_3$/MCM-41

**$N_2$ sorption isotherms**

The $N_2$ adsorption–desorption isotherms of pure MCM-41 and $TPA_3$/MCM-41and $TSA_3$/MCMC-41 are shown in Figure 26 (a). All the $N_2$ adsorption–desorption isotherms are of type IV in nature according to the IUPAC classification and exhibited an H1 hysteresis loop which is a characteristic of mesoporous solids [29]. The adsorption branch of each isotherm showed a sharp inflection, which means a typical capillary condensation within uniform pores. The position of the inflection point is clearly related to the diameter of the mesopore, and the sharpness of this step indicates the uniformity of the mesopore size distribution. The Figure 26(b) shows that all the samples have narrow pore size distribution within the mesopore range.

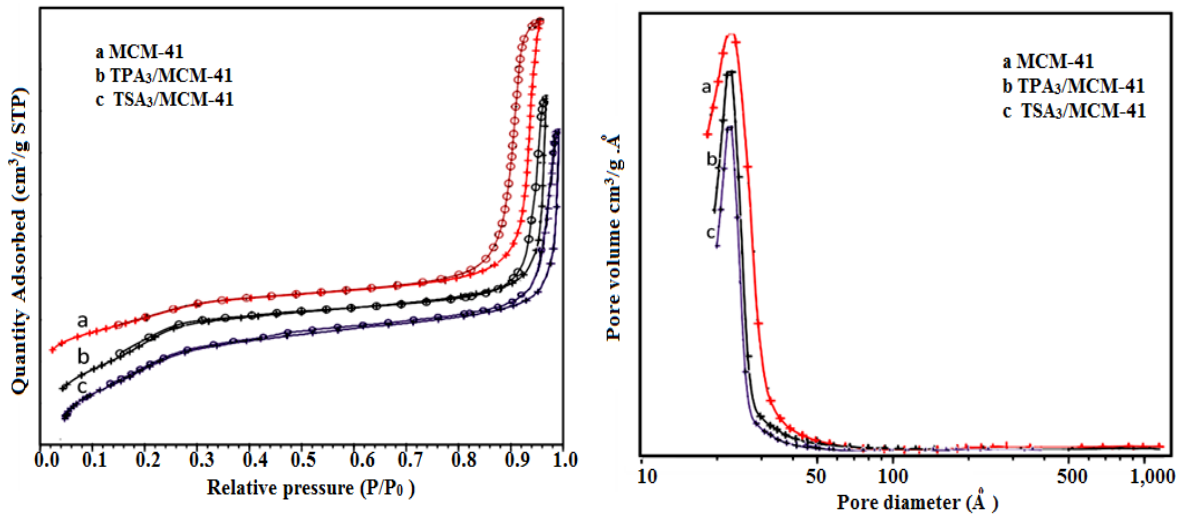


(a) (b)

**Figure 26.** (a)Nitrogen sorption isotherms of MCM-41, $TPA_3$/MCM-41 and $TSA_3$/MCM-41 (b) pore size distribution.

The values of surface area, pore size and pore volumes of support and the catalysts are presented in Table 8 and 9. Specific surface area, porosity and pore diameter, all strongly decreased for TPA/TSA containing catalysts relative to MCM-41. As the HPA loading increases surface area, pore diameter and pore volume all strongly decreases. The reason being, as the HPA species will enter the mesopores it

decrease the pore diameter, and also probably some HPA species will appear in the mesoporous channels that decrease the average pore volume as well as the surface area.

**Table 8.** Textural properties of support and catalysts.

| Catalyst | Surface area ($m^2/g$) | Pore diameter d(Å) | Mesopore volume($cm^3/g$) |
|---|---|---|---|
| MCM-41 | 659 | 47.90 | 0.79 |
| $TPA_1$/MCM-41 | 400 | 30.69 | 0.55 |
| $TPA_2$/MCM-41 | 372 | 30.53 | 0.50 |
| $TPA_3$/MCM-41 | 360 | 30.13 | 0.50 |

**Table 9.** Textural properties of support and catalysts.

| Catalyst | Surface area ($m^2/g$) | Pore diameter d(Å) | Mesopore volume($cm^3/g$) |
|---|---|---|---|
| MCM-41 | 659 | 47.9 | 0.79 |
| $TSA_1$/MCM-41 | 539.29 | 29.62 | 0.39 |
| $TSA_2$/MCM-41 | 464.16 | 29.45 | 0.30 |
| $TSA_3$/MCM-41 | 349.26 | 29.23 | 0.26 |

**$^{31}$P MAS- NMR studies**

$^{31}$P NMR is the most important method to study chemical environment around the phosphorous in heteropoly compounds. The $^{31}$P NMR spectra of TPA, $TPA_2$/MCM-41 and $TPA_3$/MCM-41 are shown in Figure 27. The pure TPA shows single peak at -15.626 ppm and is in good agreement with the reported one [25].

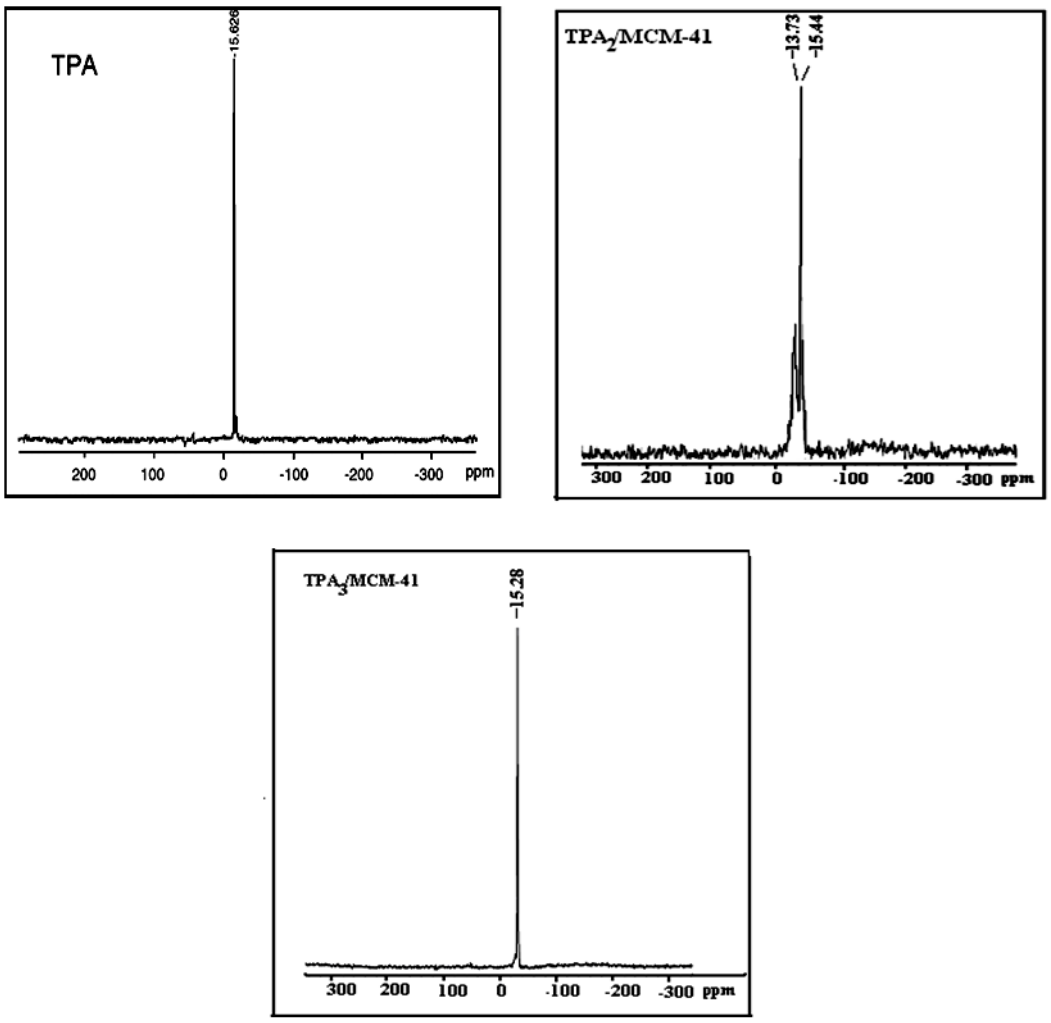


**Figure 27.** $^{31}$P MAS-NMR of TPA, $TPA_2$/MCM-41 and $TPA_3$/MCM-41

The $^{31}$P NMR spectra of $TPA_2$/MCM-41, shows two peaks one at -15.44 ppm and another peak of lower intensity at -13.3 ppm. The peak at -15.44 ppm is as expected and is in good agreement with the reported one [30]. Another peak at -13.3 ppm might indicate that the part of Keggin structure was deformed or distorted due to the strong interactions with the support, but the fundamental Keggin structure was

preserved. The results are in good agreement with the earlier reported one [30]. As there were presence of two different structures of heteropolyacid inside the mesopores of MCM-41, $TPA_2$/MCM-41 was not selected for carrying out detailed catalytic studies.

The $^{31}P$ NMR spectra of $TPA_3$/MCM-41 shows single peak at -15.523 ppm. No appreciable change in chemical shift value reveals that the surrounding environment for the supported TPA does not change when anchored to MCM-41 surface. In other words the Keggin ion structure is retained after anchoring to MCM-41. Hence $TPA_3$/MCM-41 was selected for detailed catalytic studies.

**$^{29}$Si MAS- NMR studies**

$^{29}$Si MAS-NMR is the most important method to study chemical environment around the silicon nuclei in mesoporous silica materials. Figure 28 shows the $^{29}$Si MAS-NMR spectra of the MCM-41, $TPA_3$/MCM-41, TSA and $TSA_3$/MCM-41. $^{29}$Si NMR of pure TSA shows a single peak at -84.7 ppm. A broad peak between -90 and -125 ppm was observed which can be attributed to three main components with chemical shifts at -93, -103 and -110ppm. These signals are resulted from $Q^2$(-93ppm) , $Q^3$ (-103ppm) and $Q^4$ (-110ppm) silicon nuclei, where $Q^x$ corresponds to a silicon nuclei with x siloxane linkages, i.e., $Q^2$ to disilanol Si-$(O\text{-}Si)_2(\text{-}O\text{-}X)_2$, where X is H or TPA , $Q^3$ to silanol (X-O)-Si-$(O\text{-}Si)_3$ and $Q^4$ to Si-$(O\text{-}Si)_4$ in the framework [ 31-32].

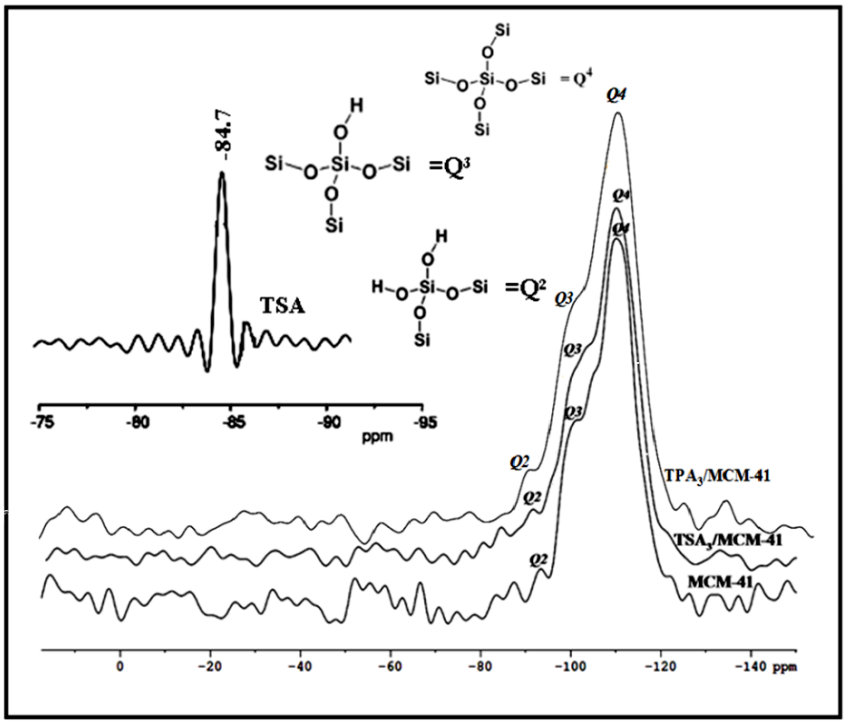


**Figure 28.** $^{29}$Si MAS-NMR spectra of MCM-41, TSA, $TPA_3$/MCM-41 and $TSA_3$/MCM-41

The spectra of $TPA_3$/MCM-41 and $TSA_3$/MCM-41 were relatively broad as compared to MCM-41 which may be due the presence of TPA/TSA. Also the intensity of the $Q^2$ and $Q^3$ peaks decreases when the support, MCM-41 is loaded with TPA/TSA .i.e., in catalysts $TPA_3$/MCM-41 and $TSA_3$/MCM-41 respectively. This reveals that MCM-41 mesoporous structure may be perturbed due to the presence of TSA inside the hexagonal channels.

**Table 10.** $^{29}Si$ MAS-NMR data of MCM-41 and $TSA_3$/MCM-41

| Catalyst | $^{29}Si$ MAS-NMR data | | | |
|---|---|---|---|---|
| | $Q^4$% | $Q^3$% | $Q^2$% | $(Q^3+Q^2)/Q^4$ |
| MCM-41 | 73 | 23 | 36 | 0.37 |
| $TPA_3$/MCM-41 | 69.5 | 26.2 | 4.3 | 0.44 |
| $TSA_3$/MCM-41 | 67.5 | 28 | 4.5 | 0.48 |

The fractions of $Q^2$, $Q^3$ and $Q^4$ units and their relative values were derived from the Figure 28 are given in Table 10. If the values of $(Q^3+Q^2)/Q^4$ for MCM-41 and $TSA_3$/MCM-41 were compared, the greater value obtained for $TPA_3$/MCM-41, $TSA_3$/MCM-41 catalyst indicates strong interaction between MCM-41 frameworks with TPA/TSA.

To study the dispersion of TPA/TSA species into MCM-41, materials were further characterized for XRD, SEM and TEM.

**X-ray diffraction (XRD)**

The XRD patterns of pure TPA, TSA, MCM-41, $TPA_3$/MCM-41 and $TSA_3$/MCM-41 are shown in figure 29. The XRD pattern of the calcined MCM-41 showed a sharp peak around $2\theta=2^o$ and few weak peaks in $2\theta=3\sim5^o$, which indicated well-ordered hexagonal structure of MCM-41.

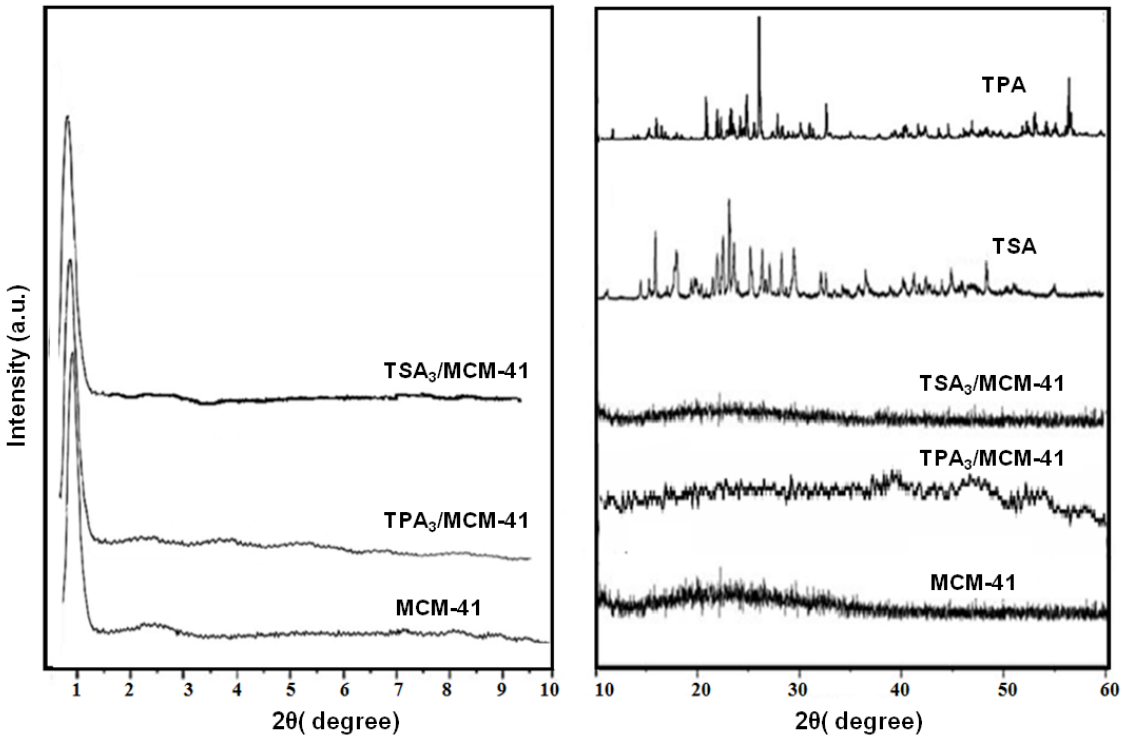


**Figure 29.** XRD patterns of pure TPA, TSA, MCM-41, $TPA_3$/MCM-41 and $TSA_3$/MCM-41

No separate crystal phase of TPA/TSA was observed in the $TPA_3$/MCM-41 and $TSA_3$/MCM-41 respectively. Further the absence of characteristic peaks of crystalline phase of TPA/TSA indicates that TPA/TSA is finely dispersed inside the hexagonal channels of MCM-41 [33]. Hence, there must be some chemical interaction between the host MCM-41 and the guest TPA/TSA.

**Scanning Electron Microscopy (SEM)**

Figure 30 (a), (b) and (c) shows the SEM image of MCM 41, $TPA_3$/MCM-41 and $TSA_3$/MCM41 respectively. The surface morphology of the anchored catalysts is almost identical to that of pure MCM-41. No change in surface morphology of the catalysts indicates TPA/TSA species are well dispersed inside the hexagonal pores. Further no separate crystallites of bulk phase of TPA/TSA were found in catalyst.

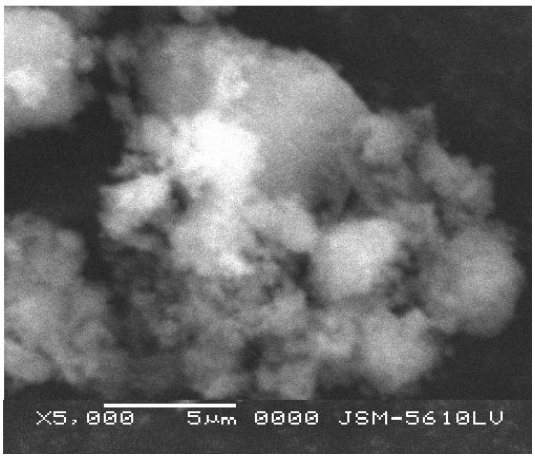


(a)MCM 41

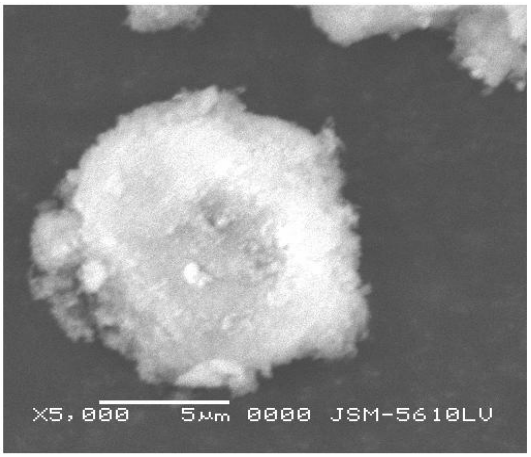


(b) $TPA_3$/MCM41

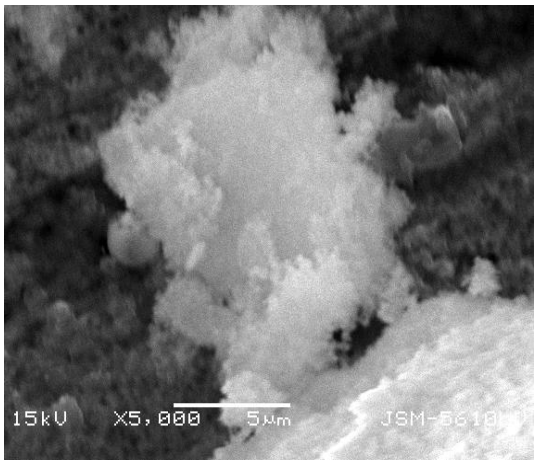


(c) $TSA_3$/MCM41

**Figure 30.** SEM images of (a) MCM 41 and (b) $TPA_3$/MCM41 (c) $TSA_3$/MCM41

**Transmission Electron Microscopy (TEM)**

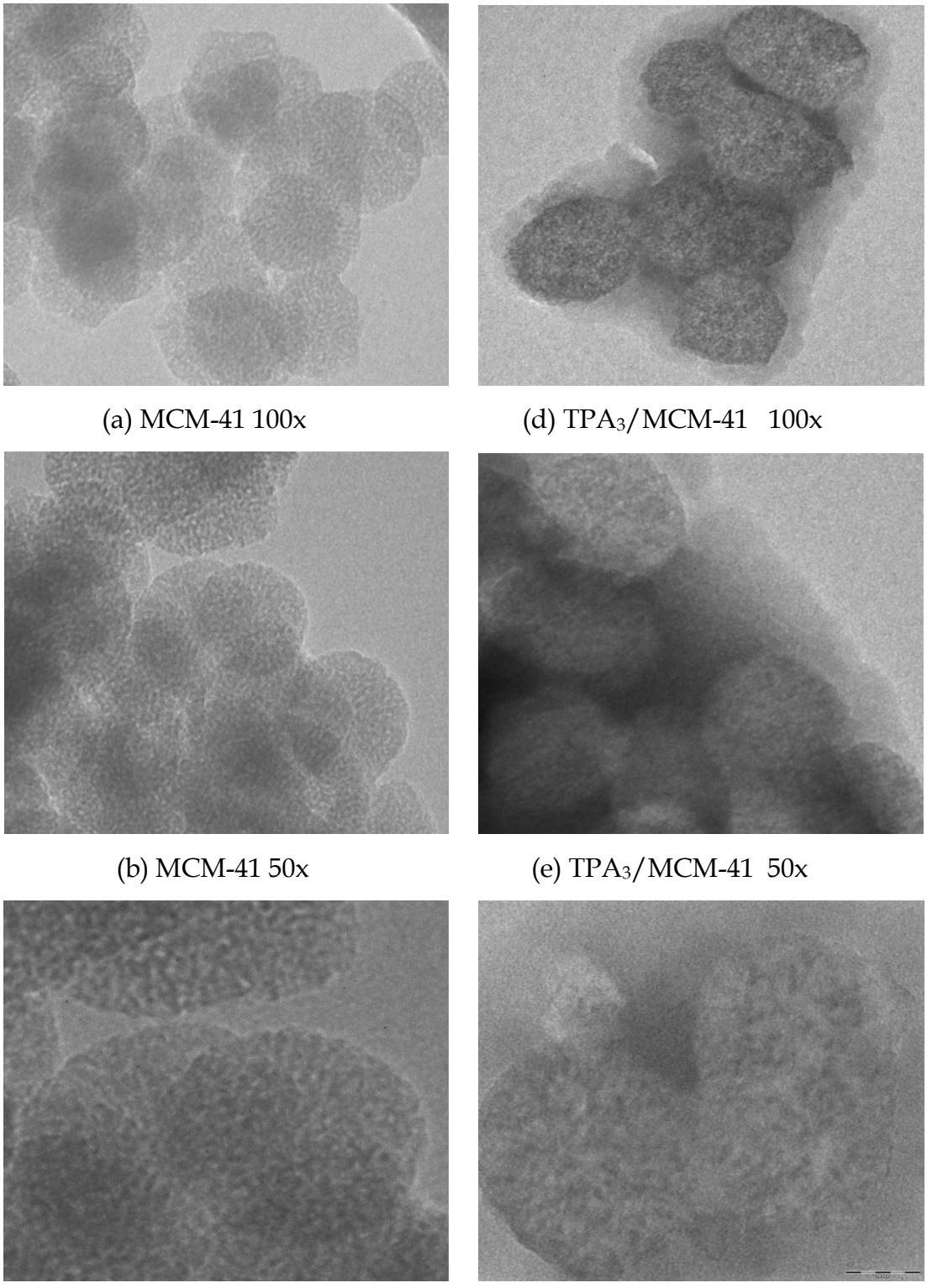

(a) MCM-41 100x (d) $TPA_3$/MCM-41 100x

(b) MCM-41 50x (e) $TPA_3$/MCM-41 50x

(c)MCM-41 20x (f) $TPA_3$/MCM-41 20x

**Figure 31.** TEM of MCM41 (a, b, c) and $TPA_3$/MCM-14 (d, e, f)

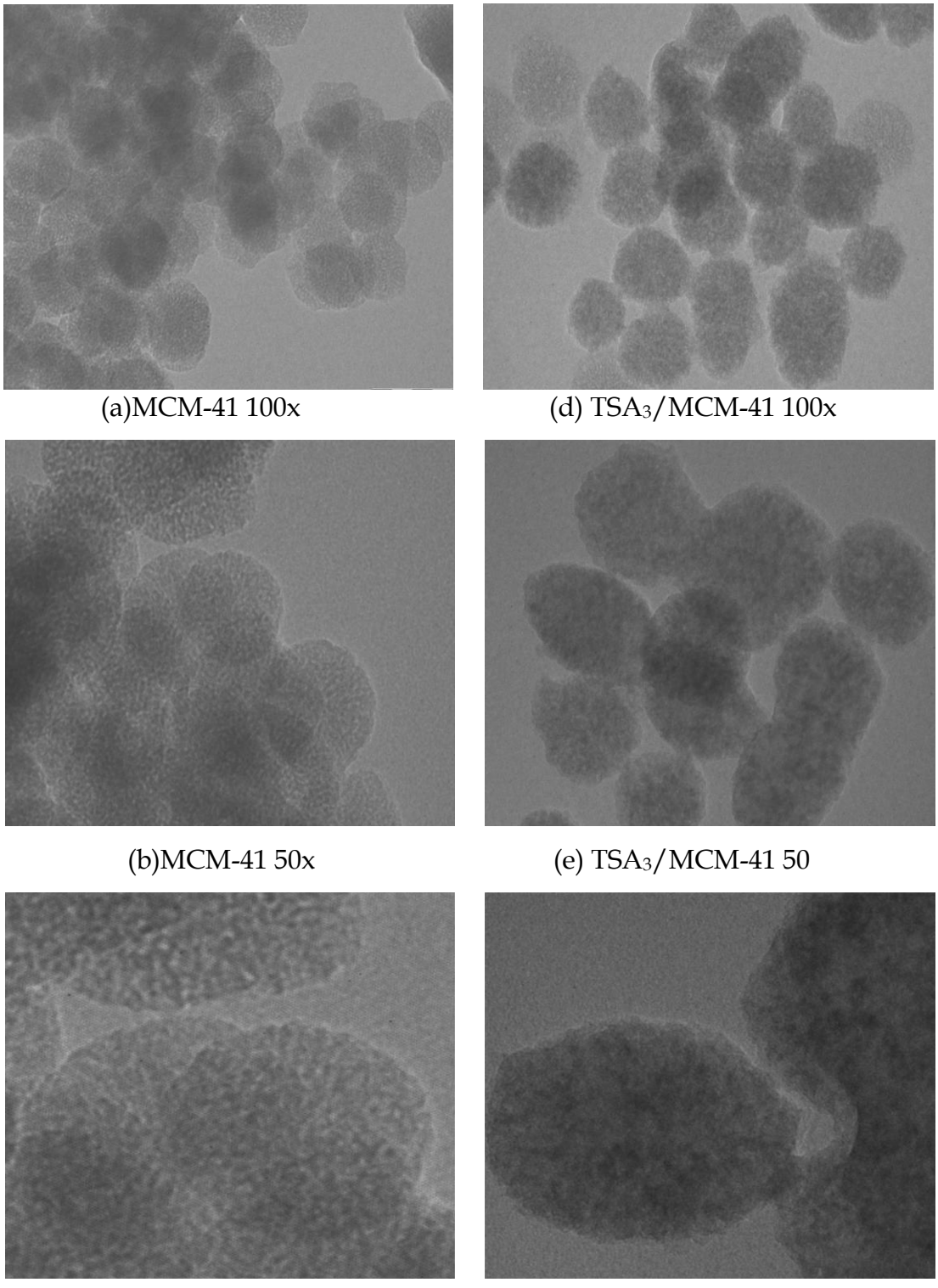

(a)MCM-41 100x (d) $TSA_3$/MCM-41 100x

(b)MCM-41 50x (e) $TSA_3$/MCM-41 50

(c)MCM-41 20x (f) $TSA_3$/MCM-41 20x

**Figure 32.** TEM of MCM-41 (a, b, c) $TSA_3$/MCM-41(d, e, f)

Figure 31 and 32 shows the TEM image of MCM 41, $TPA_3$/MCM41 and $TSA_3$/MCM41 respectively. Figure 32(a, b, c) clearly shows hexagonal mesopores in MCM-41. The TEM images of $TPA_3$/MCM41 (figure 31 d, e, f) $TSA_3$/MCM41 (Figure 32 d, e, f) shows that most of the hexagonal pores are covered with dark coloured fine particles. This indicates uniform dispersion of TPA/TSA inside the hexagonal pores of MCM-41. Other possibility is that TPA/TSA has formed very small (nm) crystals in these channels.

**Acidity measurements**

**(a) Total acidity**

Total acidity values for all the catalysts are presented in Table 11 and 12. Total acidity values indicate that MCM-41 is fairly acidic. As the HPA (TPA/TSA) loadings increases acidity values also increase and the results are as expected.

**Table 11.** Total acidity values of TPA/MCM-41 series of catalysts.

| Catalyst | Total acidity (mmol/g) |
|---|---|
| MCM-41 | 0.82 |
| $TPA_1$/MCM-41 | 1.28 |
| $TPA_2$/MCM-41 | 1.32 |
| $TPA_3$/MCM-41 | 1.41 |
| $TPA_4$/MCM-41 | 1.48 |

**Table 12.** Total acidity values of TSA/MCM-41 series of catalysts.

| Catalyst | Total acidity (mmol/g) |
|---|---|
| MCM-41 | 0.82 |
| $TSA_1$/MCM-41 | 1.14 |
| $TSA_2$/MCM-41 | 1.21 |
| $TSA_3$/MCM-41 | 1.33 |
| $TSA_4$/MCM-41 | 1.37 |

**(b)Determination of acidic strength**

According to Vasquez et al [34], the potentiometric titrations with 0.05 N n-butyl amine enable the quantitative determination of Bronsted acid sites. As suggested by Vasquez et al, sites at potential > 100mV are very strong sites, sites at mV 0< E<100 are strong and those at -100<E<0 are weak.

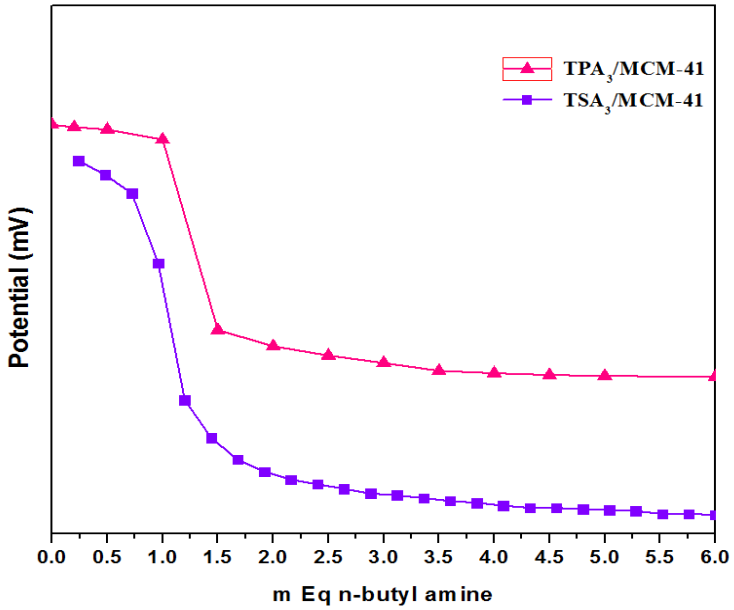


**Figure 33.** Potentiometric titration of $TPA_3$/MCM-41 and $TSA_3$/MCMC-41

From the plot shown in figure 33, an equivalent mass of 1.44 and 1.2 mg n-butyl amine was determined for $TPA_3$/MCM-41 and $TSA_3$/MCM-41 respectively at potential above 100 mV, corresponding to HPA (TPA/TSA) acidic protons and indicating that all those sites were very strong.

Moreover, according to the data (Table 11) 0.82 and 1.41 mmol/g n-butyl amine adsorbs onto support MCM-41 and $TPA_3$/MCM-41, respectively. Thus, 0.3 g TPA in 1 g of $TPA_3$/MCM-41 is equal to 0.104 mmol/g of acid. Therefore, the maximal value which can be obtained in the course of titration of this samples by n-butyl amine may be about 0.104x3(amount of protons) = 0.312 mmol/g. However, 1.41-0.82= 0.59 mmol/g. This is an ideal situation but practically it is not so when it comes to real system.

**Synthesis and Characterization of Pore expanded MCM-41 (PE-MCM-41)**

MCM-41 materials are promising supports in applications requiring large pores because of their well-defined mesoporous structure in combination with a high surface area. The typically attainable pore diameter of about 35 Å, however, is still too small for some applications. Different methods have been published by which materials with an ordered hexagonal pore system and pore diameters up to 50 Å, can be generated [35]. Due to the significantly larger pore diameter, bigger molecules can diffuse inside the pore structure of MCM-41, thereby making the catalytically active sites available for reaction.

To study the effect of support pore diameter pore expanded MCM-41 was synthesized using auxiliary organic molecule such as mesitylene. The templating micelles are enlarged by adding an organic swelling agent (mesitylene) to the CTAB surfactant (figure 34).

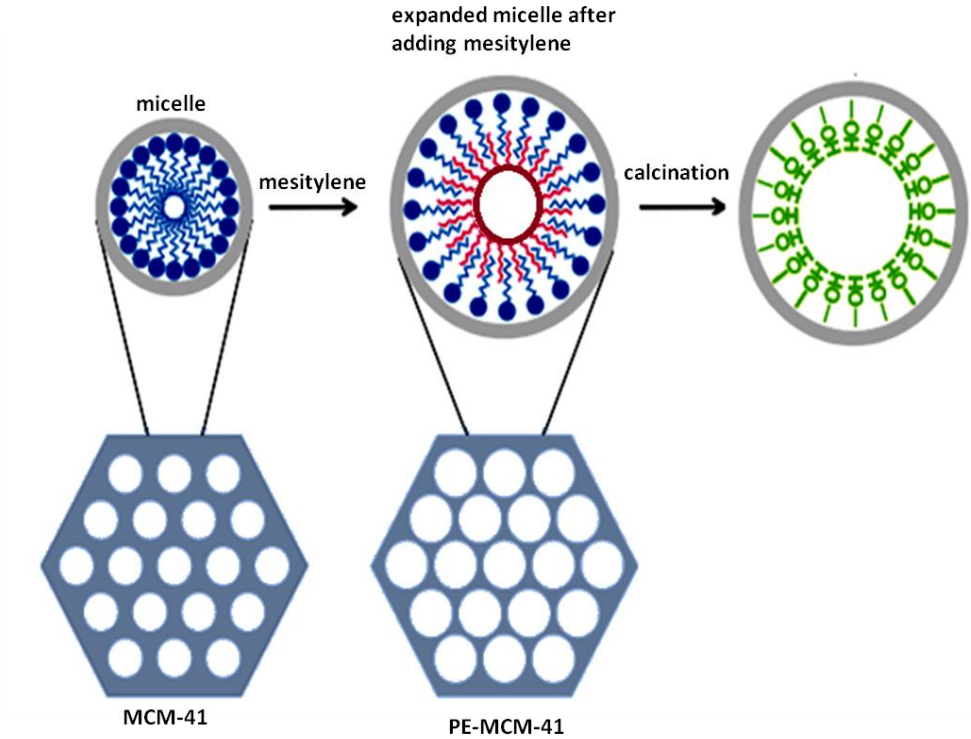


**Figure 34.** Synthesis of pore expanded MCM-41.

**Synthesis**

Pore expanded MCM-41 was synthesized using reported procedure [36] with slight modification. CTAB (4.38 g) was dissolved in 200 g of distilled water containing 1.10 g of NaOH. While the surfactant solution was stirred vigorously, 15.22 g of TEOS was added quickly. Then 10 mL mesitylene and 5 mL hexane were added to the mixture as pore-expanders. The mixture turned white within 5 seconds and was stirred for 24 h at room temperature, followed by aging at 100 °C for an additional 24 h without stirring. The resulting product was filtered, washed with distilled water, dried at room temperature. The obtained material was calcined at 555 $^{o}$C in air for 5 h. Material was designated as pore expanded MCM-41, i.e. PE-MCM-41.

**Anchoring of TPA to PE-MCM -41 (TPA/PE-MCM-41)**

TPA was anchored to PE-MCM-41 by dry impregnating method. 1 g of PE-MCM-41 was impregnated with an aqueous solution of TPA (0.3/30 g/ml of double distilled water) and dried at 100$^{o}$C for 10 h. The obtained materials were designated as $TPA_3$/PE-MCM-41.

**Characterization of PE- MCM-41 and $TPA_3$/PE-MCM-41**

PE-MCM-41 and the catalyst $TPA_3$/PE-MCM-41were characterized for FT-IR, low angle XRD, BET surface area, SEM, TEM. Samples were also characterized for total acidity. The results obtained are expected to be the same as that for MCM-41 and $TPA_3$/MCM-41 except the acidity and textural properties including surface area and pore diameter therefore we have not discussed all the techniques once again to avoid the repetitions.

**Fourier Transform Infrared Spectroscopy (FT-IR)**

FT-IR spectra of PE-MCM-41 and $TPA_3$/PE-MCM-41 are shown in figure 35. FT-IR of PE-MCM-41 (figure 35) shows a broad band around 1300-1000 $cm^{-1}$ corresponding to asymmetric stretching of Si-O-Si. The band at 801 and 458 $cm^{-1}$ are due to symmetric stretching and bending vibration of Si-O-Si respectively. The band at 966 $cm^{-1}$ corresponds to symmetric stretching vibration of Si-OH. The broad absorption band around 3448 $cm^{-1}$ is the absorption of Si-OH on surface, which provides opportunities for forming the hydrogen bond.

FT-IR spectra of $TPA_3$/PE-MCM-41 (figure 35) is almost the same as that of PE-MCM-41. The reported bands for TPA, at 1088 $cm^{-1}$, 987 $cm^{-1}$and 800 $cm^{-1}$ corresponding to W-O-W bending, W-O and P-O symmetric stretching respectively, are absent in $TPA_3$/PE-MCM-41. If TPA is dispersed onto the surface of support, the mentioned bands for TPA should be seen in the FT-IR spectra. The lack of IR-bands of TPA may be because of too low amount of acid, or the TPA bands superimposed with those of support.

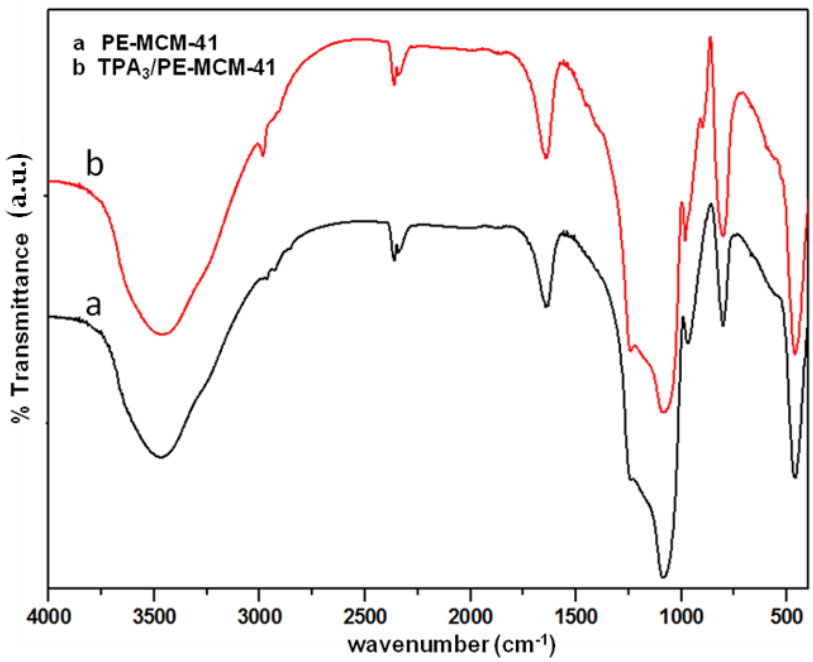


**Figure 35.** FT-IR spectra of PE-MCM-41 and $TPA_3$/MCM-41.

**X-ray diffraction (XRD)**

The XRD patterns of pure TPA, PE-MCM-41, $TPA_3$/PE-MCM-41 are shown in figure 36. The XRD pattern of the calcined PE-MCM-41 showed a sharp peak around $2\theta=2^o$ and few weak peaks in $2\theta=3\sim5^o$, which indicated well-ordered hexagonal structure of PE-MCM-41.

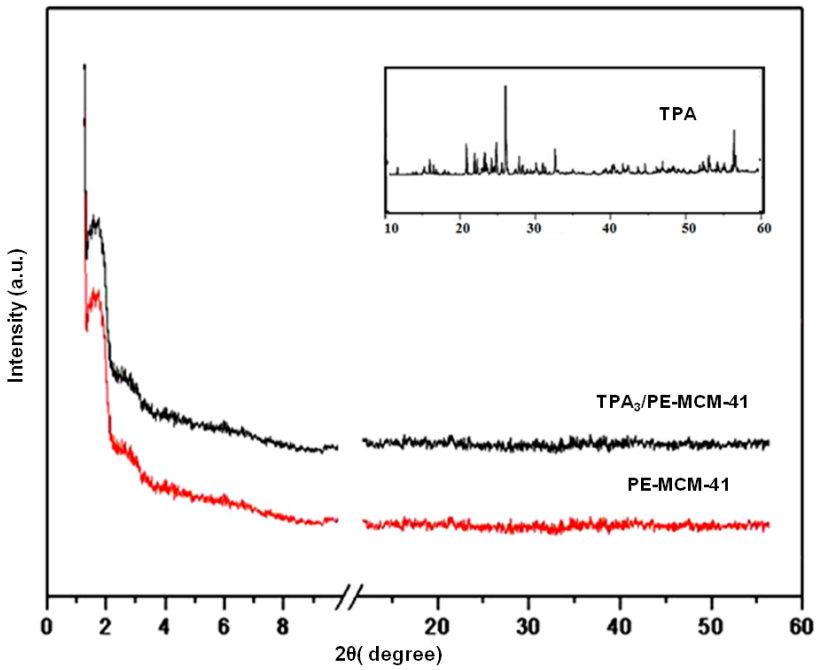


**Figure 36**. XRD patterns of PE-MCM-41 and $TPA_3$/PE-MCM-41.

No separate crystal phase of TPA was observed in the $TPA_3$/PE-MCM-41 respectively. Further the absence of characteristic peaks of crystalline phase of TPA indicates that TPA is finely dispersed inside the hexagonal channels of PE-MCM-41.

**$N_2$ sorption isotherms**

The $N_2$ adsorption–desorption isotherms of PE-MCM-41 and $TPA_3$/PE-MCM-41 are shown in figure 37 (a). All the $N_2$ adsorption–desorption isotherms are of type IV in nature according to the IUPAC classification and exhibited an H1 hysteresis loop which is a characteristic of mesoporous solids. The adsorption branch of each isotherm showed a sharp inflection, which means a typical capillary condensation within uniform pores. The position of the inflection point is clearly related to the diameter of the mesopore, and the sharpness of this step indicates the uniformity of the mesopore size distribution. The figure 37(b) shows that all the samples have narrow pore size distribution within the mesopore range.

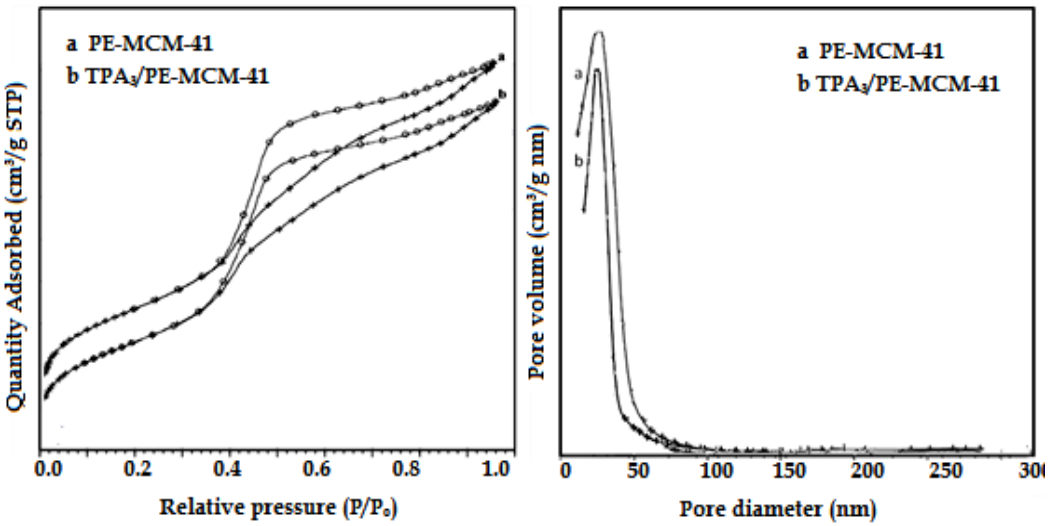


**Figure 37**. (a) Nitrogen sorption isotherm and (b) Pore size distribution of PE-MCM-41 and $TPA_3$/MCM-41.

The values of surface area, pore size and pore volumes of support and the catalysts are presented in Table 13. Specific surface area, porosity and pore diameter, all strongly decreased for $TPA_3$/PE-MC relative to PE-MCM-41. As the TPA loading increases surface area, pore diameter and pore volume all strongly decreases. The reason being, as the TPA species will enter the mesopores it decrease the pore diameter, and also probably some TPA species will appear in the mesoporous channels that decrease the average pore volume as well as the surface area.

**Table 13.** Textural properties of PE-MCM-41 and $TPA_3$/PE-MCM-41

| Material | Surface area ($m^2/g$) | pore diameter (nm) | Mesopore volume ($cm^3/g$) | Total acidity (mmol/g) |
|---|---|---|---|---|
| PE-MCM-41 | 1317 | 5.0 | 1.62 | 1.1 |
| $TPA_3$/PE-MCM-41 | 631 | 4.8 | 0.78 | 1.46 |

**Scanning Electron Microscopy (SEM)**

Figure 38 shows the SEM image of PE-MCM 41 and $TPA_3$/PE-MCM-41. The surface morphology of the anchored catalysts is almost identical to that of PE-MCM-41. No change in surface morphology of the catalysts indicates TPA species are well dispersed inside the hexagonal pores. Further no separate crystallites of bulk phase of TPA were found in catalyst.

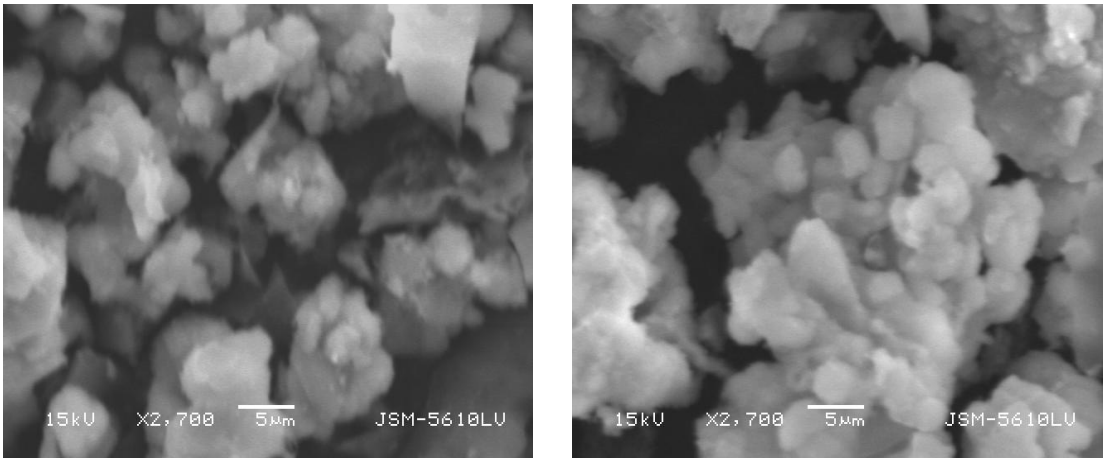


PE-MCM-41 $TPA_3$/PE-MCM-41

**Figure 38.** SEM images of PE-MCM-41 and $TPA_3$/PE-MCM-41

**Transmission Electron Microscopy (TEM).**

Figure 39 shows the TEM image of PE-MCM 41 and $TPA_3$/PE-MCM41. Figure 39 (a, c) clearly shows hexagonal mesopores in PE-MCM-41. The TEM images of $TPA_3$/PE-MCM41 (figure 39 b, d) shows that most of the hexagonal pores are covered with dark coloured fine particles. This indicates uniform dispersion of TPA inside the hexagonal pores of PE-MCM-41. Other possibility is that TPA has formed very small (nm) crystals in these channels.

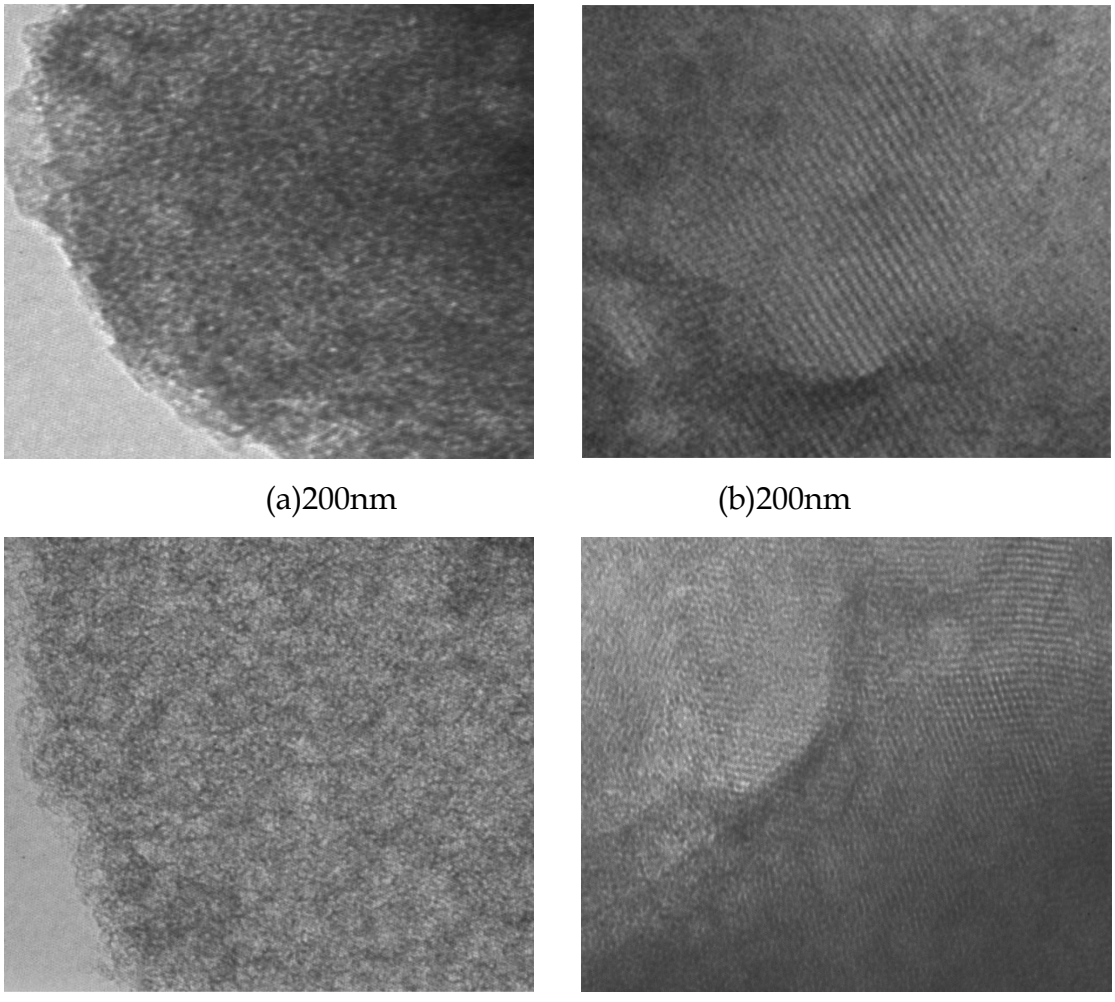

(a)200nm (b)200nm

(c)100nm (d) 100nm

**Figure 39.** TEM images of PE-MCM-41(a, c) and $TPA_3$/PE-MCM-41 (b, d)

Hence the TPA was successfully anchored to pore expanded MCM-41 and the synthesized catalyst $TPA_3$/PE-MCM-41, exhibits considerably high surface area and pore diameter as compared to that of $TPA_3$/MCM-41.

**Conclusion**

- MCM-41 was synthesized by non-hydrothermal synthetic method, and that was used for anchoring TPA/TSA. XRD and TEM confirm the formation of MCM-14 with hexagonal long range order in the material.
- Thermal stability of TPA/TSA increases after anchoring to MCM-41, and both the catalysts, $TPA_3$/MCM-41 and $TSA_3$/MCM-41 were stable up to 600 $^oC$.
- FT-IR and DRS spectra show that Keggin ion structure of TPA/TSA remains intact even after anchoring to MCM-41. $^{31}P$ MAS-NMR also confirms the retainment of Keggin structure of TPA even after anchoring to MCM-41.
- BET surface area, $^{29}Si$ NMR data and Raman studies show that there is a strong interaction, hydrogen bonding, between terminal oxygens of TPA/TSA with the surface silanol groups of MCM-41(figure 40).

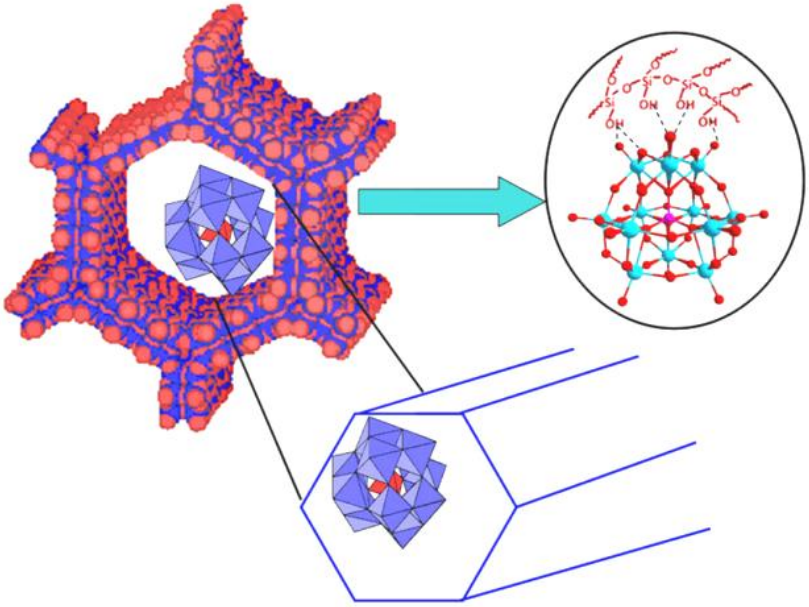

**Figure 40.** Interaction of TPA/TSA with MCM-41

- XRD, SEM, and TEM studies reveal that TPA/TSA is uniformly dispersed inside the channels without disturbing the hexagonal array of MCM-41.
- Pore expanded MCM-41 was synthesized successfully with considerably large pore diameter and high surface area as compared to MCM-41.

**References**


1. J. Perez-Pariente, I. Diaz, F. Mohino, E. Satre, *Appl. Catal. A: Gen.* 254, 173 (2003)
2. S. Shylesh, P. P. Samuel, A. P. Singh, *Micropor. Mesopor. Mater.* 100,250 (2007)
3. M. H. Lim, C. F .Branford, A. Stein, *J. Am. Chem. Soc*. *119*, 4090 (1997)
4. Q. Cai, Z.S. Luo, W. Q. Pang, Y. W Fan, X. H. Chen, F. Z. Cui, *Chem. Mater. 13*, 258 (2001)
5. R. Richards (ed.), "Surface and Nanomolecular Catalysis", CRC press, Ch 1, p2, (2006)
6. J. M. Thomas, W. J. Thomas, Principles and Practice of Heterogeneous Catalysis, VCH, Weinheim, (1997)
7. R. A. van Santen, P. W. N. M. Van Leeuwen, J. A. Moulijin, B. A. Averil (Eds.), Catalysis: An Integrated Approach, (2nd ed.), Elsevier, Amsterdam(1999)
8. "Spectroscopic Characterization of Heterogeneous Catalysts", J. L. G. Fierro, *Stud. Surf. Sci. Cat.*, Elsevier, vol 57A (1990)
9. D. Skoog, F. Holler, T. Nieman, "Principles of Instrumental Analysis", 5th ed., (2001)
10. J. H. Clark, A. P. Kybett, D. J. Maequarrie, "Supported reagents: preparation, analysis and application", VCH Inc. New York (1992).
11. D. J. Gardiner, Practical Raman spectroscopy. Springer-Verlag (1989).
12. N. Gupta, V. Kartha, R. Rajadhyaksha, "Spectroscopic methods in heterogeneous catalysis", Tata McGraw Hill, (1989)
13. J. Mayer, L. A. Giannuzzi, T. Kamino, J. Michael. TEM Sample Preparation and FIB-Induced Damage. Mrs Bulletin, vol 32 (2007)
14. B. Viswanathan, S. Sivasanker, A. V. Ramaswamy , "Catalysis: principles and applications", (Eds.), Norsa, New Delhi (2002)
15. K. Mohan Reddy, N. Lingaiah, P. S. Sai Prasad, and I. Suryanarayana, *J. Solution. Chem*. 35 , 407 (2006)
16. H. R .Sahu, G. R .Rao. *Bull. Mater. Sci*. 23, 349 (2000)

17. L. A.M .Cardoso, Jr. W. Alves., A. R.E .Gonzaga, L. M. G. Aguiar, H. M.C Andrade, *J. Mol. Catal. A: Chem.*209, 189 (2004)
18. J.S. Beck, J.C. Vartuli, W.J. Roth, M.E. Leonowicz, C.T. Kresge, K.D. Schmit, C.T.W. Chu, D.H. Olson, E.W. Sheppard, S.B. McCullen, J.B. Higgins, J.L. Schlenker, *J. Am.Chem. Soc.* 114, 10834 (1992).
19. C.T. Kresge, M.E. Leonowicz, W.J. Roth, J.C. Vartuli, J.C. Beck, *Nature*. 359, 710 (1993)
20. G. D. Yadav, V. V. Bokade, *Appl. Catal. A*. 147, 299 (1996)
21. C. Rocchiccioli-Deltcheff, *Inorg. Chem.* 22, 207 (1983)
22. G. Kamalakar; K. Komura, Y. Kubota, Y. Sugi, *J. Chem. Technol. Biotechnol. 81*, 981 (2006)
23. T. Okuhara, N. Mizuno, *M. Misono, Adv. Catal.* 41, 113 (1996)
24. B. Jermy, A. Pandurangan, *Appl. Catal. A. Gen.* 295, 185 (2005)
25. T. Okuhara, N. Mizuno, M. Misono, *Adv. Catal*. 41 ,113 (1996)
26. C. Rocchiccioli-Deltcheff, M. Fournier, R. Franck, R. Thouvenot. *Inorg.Chem*. 22, 207 (1983)
27. A. Thomas, C. Dablemont, J. M. Basset, F. C. R. Lefebvre, *Chim*., 8, 1969 (2005)
28. M. T. Pope, Heteropolyacid and Isopolyoxometallates; Sringer- Verlag: Berlin, (1983).
29. Y. Luo, Z. Hou, R. Li, X. Zheng, *Micropor. Mesopor. Mater.* 109, 585 (2008)
30. L.F. Chena, J.A. Wanga, L.E. Noren, J. Aguilarb, J. Navarretec, P. Salasc, J.A. Montoyac, D. Angel, *J. of Solid State Chem.*, 180, 2958 (2007)
31. R.C. Schroden, C.F. Blanford, B.J. Melde, B.J.S. Johnson, A. Stein, *Chem. Mater*. 13 ,1074 (2001)
32. W.H. Zhang, J. Lu, B. Han, M. Li, J. Xiu, P. Ying, C. Li, *Chem. Mater*. 14, 3413 (2002)
33. A.E. Rahman ,S. Khdera, H. M.A. Hassana, M. S. El-Shall, *Appl Catal A: Gen*. 411– 412, 77(2012)
34. P. Vazquez, L. Pizzio, C. Caceres, M. Blanco, H. Thomas, E. Alesso, L. Finkielsztei, L. Lantano, G. Moltrasio, J. Aguirre, *J. Mol. Catal. A: Chem.* 161, 223 (2000)

35. B. Lindlar, M. Luchinger, A. Rothlisberger, M. Haous, G. Pirngruber, A Kogelbauer, R. Prins, *J. Mater. Chem.* 12, 528 (2002)
36. M. H. Lim, A. Stein, *Chem. Mater*. 11, 3285 (1999)